AD-A012 867

TRANSPASSIVE DISSOLUTION

Ken Nobe

California University

Prepared for:

Office of Naval Research

May 1975

UCLA-ENG-7539
MAY 1975

TRANSPASSIVE DISSOLUTION

KEN NOBE, Principal Investigator

SECURITY CLASSIFICATION OF THIS PAGE (When Data Entered)

REPORT DOCUMENTATION PAGE		READ INSTRUCTIONS BEFORE COMPLETING FORM
1. REPORT NUMBER UCLA - ENG - 7539	2. GOVT ACCESSION NO.	3. RECIPIENT'S CATALOG NUMBER
4. TITLE (and Subtitle) TRANSPASSIVE DISSOLUTION		5. TYPE OF REPORT & PERIOD COVERED Final, 1970 - 1975 6. PERFORMING ORG. REPORT NUMBER
7. AUTHOR(s) Ken Nobe		8. CONTRACT OR GRANT NUMBER(s) N00014 - 69 - A - 0200 - 4029
9. PERFORMING ORGANIZATION NAME AND ADDRESS School of Engineering and Applied Science University of California, Los Angeles, CA 90024		10. PROGRAM ELEMENT, PROJECT, TASK AREA & WORK UNIT NUMBERS ONR NR 036 - 088
11. CONTROLLING OFFICE NAME AND ADDRESS Office of Naval Research U.S. Department of the Navy Arlington, VA		12. REPORT DATE May 1975 13. NUMBER OF PAGES 69
14. MONITORING AGENCY NAME & ADDRESS(if different from Controlling Office)		15. SECURITY CLASS. (of this report) Unclassified 15a. DECLASSIFICATION/DOWNGRADING SCHEDULE N-A

16. DISTRIBUTION STATEMENT (of this Report)

This document approved for public release and sale; distribution unlimited.

17. DISTRIBUTION STATEMENT (of the abstract entered in Block 20, if different from Report)

18. SUPPLEMENTARY NOTES

To be presented at fall meeting of the Electrochemical Society, Dallas, Texas, October 5 - 10, 1975

19. KEY WORDS (Continue on reverse side if necessary and identify by block number)

Localized Corrosion
Pitting Corrosion
Crevice Corrosion
Corrosion Kinetics

20. ABSTRACT (Continue on reverse side if necessary and identify by block number)

The rate of iron and nickel dissolution in dilute and concentrated acidic chloride solutions has been investigated with the rotating disk electrode technique. In dilute solutions OH^- and Cl^- accelerate the rates of both iron and nickel dissolution. The empirical rate expression for nickel is

DD FORM 1 JAN 73 1473 EDITION OF 1 NOV 65 IS OBSOLETE
S/N 0102-014-6601

PRICES SUBJECT TO CHANGE

SECURITY CLASSIFICATION OF THIS PAGE (When Data Entered)

$i_{Ni} = k_{Ni}(OH^-)^{0.5}(Cl^-)^{0.5} \exp(F\varphi/RT)$. The rate expression for iron is $i_{Fe} = k_{Fe}(OH^-)^{0.6}(Cl^-)^{0.4} \exp(3F\varphi/4RT)$, at low polarization, and $i'_{Fe} = k'_{Fe}(OH^-) \exp(3F\varphi/2RT)$ at high polarization.

In concentrated solutions, both iron and nickel are accelerated by H^+ and Cl^-, and the empirical rate expressions are $i_{Fe} = k_{Fe}[H^+][Cl^-] \exp(F\varphi/2RT)$ and $i_{Ni} = k_{Ni}[H^+]^{0.6}[Cl^-]^{1.3} \exp(F\varphi/RT)$. For high H^+ - very low Cl^- concentrations, iron dissolution is inhibited by chloride ions and the empirical rate of iron dissolution at constant H^+ can be expressed by $i_{Fe} = k_{Fe}[Cl^-]^{-\delta} \exp[(3/2 - \delta)F\varphi/RT]$ where δ changes from 0 to 1 with increasing Cl^-.

Mechanisms for both iron and nickel dissolution in dilute and concentrated acid chloride solution consistent with the experimental results have been proposed.

UCLA - ENG - 7539
MAY 1975

FINAL REPORT

TRANSPASSIVE DISSOLUTION

GRANT NO. N00014-69-A-200-4029, NR 036-088
METALLURGY PROGRAM
OFFICE OF NAVAL RESEARCH
U.S. DEPARTMENT OF THE NAVY

Principal Investigator: Ken Nobe, Professor

SCHOOL OF ENGINEERING AND APPLIED SCIENCE
UNIVERSITY OF CALIFORNIA
LOS ANGELES, CALIFORNIA 90024

MAY 1975

TABLE OF CONTENTS

PART I

NICKEL DISSOLUTION IN DILUTE AND CONCENTRATED ACIDIC CHLORIDE SOLUTIONS

A. M. BENGALI AND KEN NOBE

ABSTRACT

The anodic dissolution of nickel in acidic chloride solutions of constant ionic strengths of 1M and 5M has been investigated. Perchloric acid and sodium perchlorate were used as supporting electrolytes. By maintaining the ionic strength constant at either 1M or 5M, the effect of H^+ and Cl^- on nickel dissolution was determined by varying the respective concentrations systematically. For Cl^- and H^+ less than 1M, both OH^- and Cl^- accelerate nickel dissolution. The empirical rate equation for nickel dissolution in lower concentrations of acid chloride solutions, $i_{a,OH}$, has been determined as:

$$i_{a,OH} = k_{a,OH} (Cl^-)^{0.5} (OH^-)^{0.5} \exp\left(\frac{F\varphi}{RT}\right)$$

for (Cl^-) and $(H^+) < 1M$.

For H^+ concentrations greater than 1M, both H^+ and Cl^- accelerate nickel dissolution. That is, in contrast to low H^+ concentrations in which nickel dissolution increases with decreasing H^+ concentrations, the rate of nickel dissolution increases with increase in H^+ greater than 1M. Furthermore, at higher Cl^- concentrations, (>1 M), nickel dissolution is accelerated more strongly by Cl^-. The empirical rate equation for nickel dissolution in higher concentrations of acid chloride solutions, $i_{a,H}$, has been determined as

$$i_{a,H} = k_{a,H} [H^+]^{0.6} [Cl^-]^{1.3} \exp\left(\frac{F\varphi}{RT}\right)$$

for $1 \leq [H^+] \leq 5M$ and $1 \leq [Cl^-] \leq 5M$.

Mechanisms for nickel dissolution in dilute and concentrated acid chloride solution consistent with the experimental results have been proposed.

INTRODUCTION

Nickel is an important alloying element in many iron-based alloys. The anodic dissolution behavior of nickel has not been extensively studied, but the literature on its passivation behavior is voluminous. One probable reason for the dearth of kinetic studies on nickel dissolution even in acidic solutions is that oxide films readily form in the active dissolution region which makes difficult definitive electrochemical polarization measurements. In order to understand pitting and crevice corrosion of nickel and nickel-based alloys, it is important to obtain detailed information on the kinetics of nickel dissolution in highly acidic chloride solutions. This report presents the results of an investigation on the anodic dissolution of nickel in acidic solutions over a wide range of hydrogen ion and chloride ion concentrations with the ionic strength of both $HCl-HClO_4$ and HCl-NaCl solutions maintained constant at either 1 or 5M.

EXPERIMENTAL

The nickel electrodes were cut from a 1/8" diam., Ni 200 rod into 1.25" lengths. One end face of each electrode was polished on a grinding wheel with #400, followed by # 600 grit carborundum aloxite paper. The polished electrodes were cleaned with a soap solution, rinsed with distilled water and degreased with hot benzene in a Soxhlet column for four hours, annealed under vacuum ($\approx 3 \times 10^{-5}$ Torr) at $750^{o}C$ for one hour and allowed to cool slowly to room temperature. A Teflon rod, 3/8" diam., was cut into 3/4" lengths and drilled axially to an internal diameter of 3/22". The electrode was forced through this Teflon sleeve to obtain a leakproof fit. The cross-sectional area (0.083 sq. cm.) to be exposed to the solution was then polished. A schematic drawing of the rotating disk electrode and electrochemical cell is shown in Figure 1. More details of the apparatus are given elsewhere (1).

Solutions containing chloride and perchlorate ion were prepared from Analytical Reagent Grade Chemicals -- NaCl, $NaClO_4$, concentrated HCl and concentrated $HClO_4$. Deionized and distilled water was used to prepare electrolytic solutions. Prepurified grade N_2 gas which was further purified by pas-

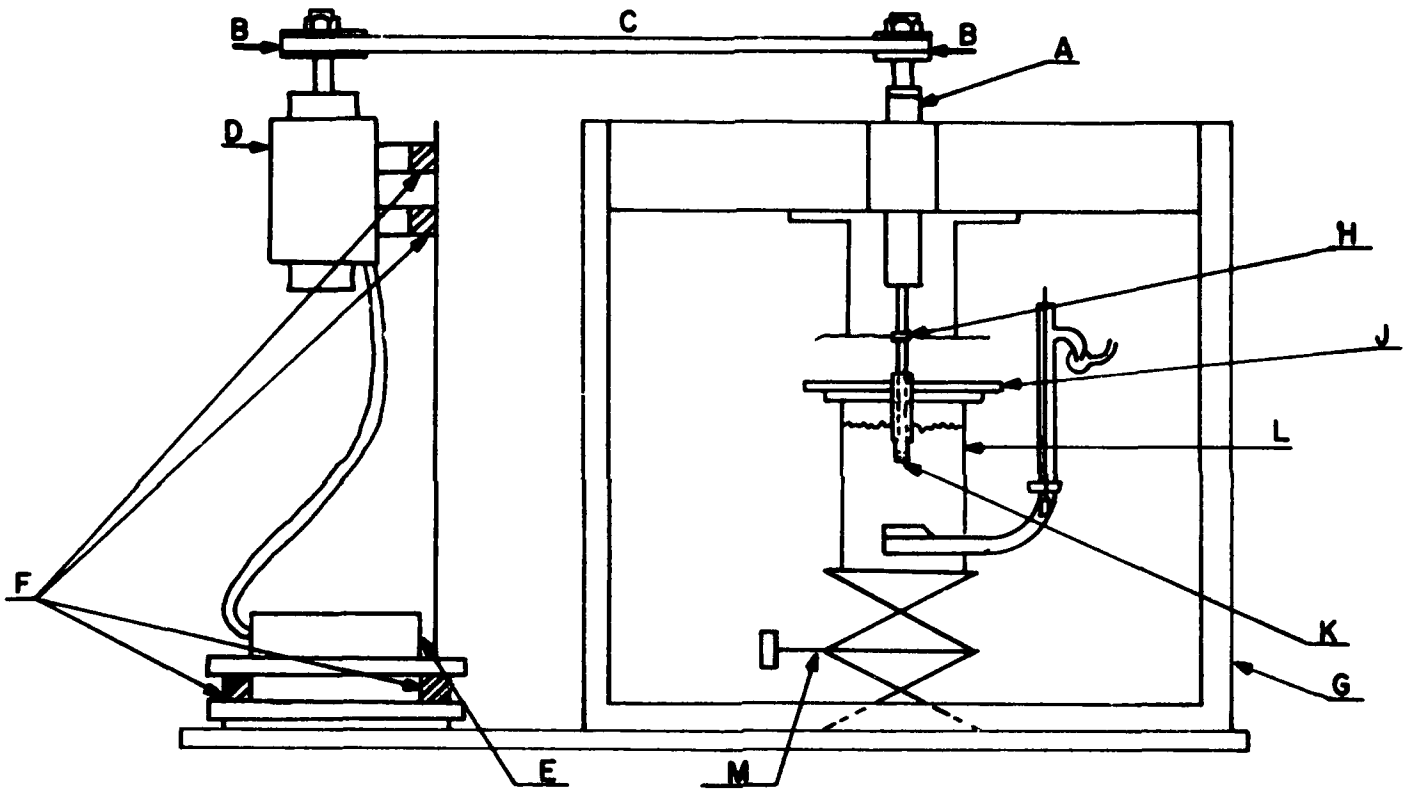

Figure 1. Rotating Disk Electrode Assembly and Test Cell

A = Quill; B = Pulleys; C = Belt; D = D.C. motor; E = Variable speed control; F = Rubber vibration mounts; G = Steel frame; H = Brass slip-ring and contact; J = PVC plate; K = Test electrode surface; L = Glass cell; M = Mounting jack.

sage through a Vycor glass column containing copper filings heated to a temperature of $\approx$ 450°C, was used to deoxygenate the electrolyte. The Cu column was periodically reactivated by passing through H_2 gas at $\approx$ 250°C.

A saturated calomel electrode (S. C. E.) served as the reference electrode. A salt-bridge containing a solution of 4.2M NaCl separated the reference electrode from the electrolyte. This bridge was necessary since a $KClO_4$ precipitate would form on the fiber tip of the reference electrode if it was in direct contact with ClO_4^- solution causing periodic fluctuating potentials.

Polarization measurements were made with an Anotrol Linear Scan Generator unit (Model 4510) was used in conjunction with the Potentiostat to carry out linear potential sweeps. The current and potential signals were recorded simultaneously on a Moseley X-Y recorder (Model 7035 A).

Test electrodes were activated before immersing it in the electrolyte prior to each experiment. Activation procedures were necessary to ensure reproducible results in a given electrolyte system. The best method of activation was determined by trial and error. For the 1M HCl-NaCl electrolytes the best reproducibility was obtained when electrodes were activated in 5N HCl solution for 15 minutes before immersion in the electrolyte and, then, cathodically pre-polarized for 3 minutes at $\approx$ 100 mA/cm^2. For the 1M HCl-$HClO_4$ electrolytes, the activation procedure consisted of only consisted of only cathodic pre-polarization for 3 minutes at $\approx$ 100 mA/cm^2. There were no activation procedures performed for either the 5M HCl-NaCl or 5M HCl-$HClO_4$ electrolytes.

After activation the electrode usually reached a steady-state rest (corrosion) potential within an hour. Subsequently, polarization measurements were performed at various rotation rates, potential sweep rates, and hydrogen ion and chloride ion concentrations.

RESULTS

All potential values presented in this report are corrected for the liquid junction potentials. At the end of each experiment the nickel surface was examined under a microscope. When the test electrolyte contained chloride ions, the electrode surface was typically characterized by localized corrosion, resulting in the formation of pits. The size and number of pits increased with increasing chloride ion concentration, but were generally unaffected by changes in H^+ ion concentration. On the other hand, when there was absence of chloride ions in the test electrolyte, or when $(Cl^-) << (ClO_4^-)$, the nickel surface was dull and uniformly etched, without any appearance of pits.

1. Effect of H^+ in 1M Cl^- Solutions (pH = 0.05 - 2.0).

a. Corrosion potentials: The corrosion potentials which attained steady state values within one hour are presented in Table 1. This steady state value was observed to be independent of rotation speed up to 7000 rpm and dependent on (H^+) as:

$$\frac{\partial \varphi_{corr}}{\partial \log (H^+)} = 0.050 \text{ V} \qquad (1a)$$

b. Polarization behavior: Figure 2 shows the effect of pH on the anodic polarization behavior of nickel. These curves were independent of the rotation rate up to 7000 rpm and the anodic Tafel slopes,

$$\left(\frac{\partial \varphi}{\partial \log I}\right)_{(H^+)} = 0.060 \text{ V/dec.} \qquad (1b)$$

The anodic dissolution increased with increase in pH. These anodic curves were obtained at a sweep rate of 2.5 mv/min in the pH range 0.05 to 1.5. Sweep rates faster than 2.5 mv/min did not yield Tafel behavior. However, for pH = 2.0, the potential sweep rate had to be lowered to 0.3 mv/min, in order to obtain Tafel behavior. Subsequent increase to pH = 3.0 Tafel behavior was not obtained for the active dissolution of nickel, and the electrode appeared to begin to passivate.

TABLE 1. Effect of pH on nickel dissolution in 1M Cl^- solutions

Electrolyte	pH	φ_{corr} (mv vs SCE)	Anodic Tafel Slope (mv vs dec)	i_{corr} ($\mu A/cm^2$)
1.0M HCl + 0.0M NaCl	0.0	-291± 5	60	21
0.32M HCl + 0.68M NaCl	0.5	-323± 6	60	7
0.1M HCl + 0.9M NaCl	1.0	-347± 3	60	6
0.032M HCl + 0.968M NaCl	1.5	-370± 4	60	3
0.01M HCl + 0.99M NaCl	2.0	-389± 2	60	2

TABLE 2. Effect of Cl^- on nickel dissolution in 1M H^+ solutions.

Electrolyte	$[Cl^-]$ (M)	φ_{corr} (mv vs SCE)	Anodic Tafel Slope (mv vs dec)	i_{corr} ($\mu A/cm^2$)
0.0M HCl + 1.0M $HClO_4$	0.000	-268± 5	75	5
0.01M HCl + 0.99M $HClO_4$	0.010	-264± 7	75	8
0.025M HCl + 0.975M $HClO_4$	0.025	-271± 7	75	8
0.05M HCl + 0.95M $HClO_4$	0.050	-273± 5	75	13
0.1M HCl + 0.9M $HClO_4$	0.100	-285± 3	75	12
0.25M HCl + 0.75M $HClO_4$	0.250	-285± 10	75	18
0.5M HCl + 0.5M $HClO_4$	0.500	-292± 8	75	23
0.8M HCl + 0.2M $HClO_4$	0.800	-296± 10	75	21
1.0M HCl + 0.0M $HClO_4$	1.000	-291± 5	60	21

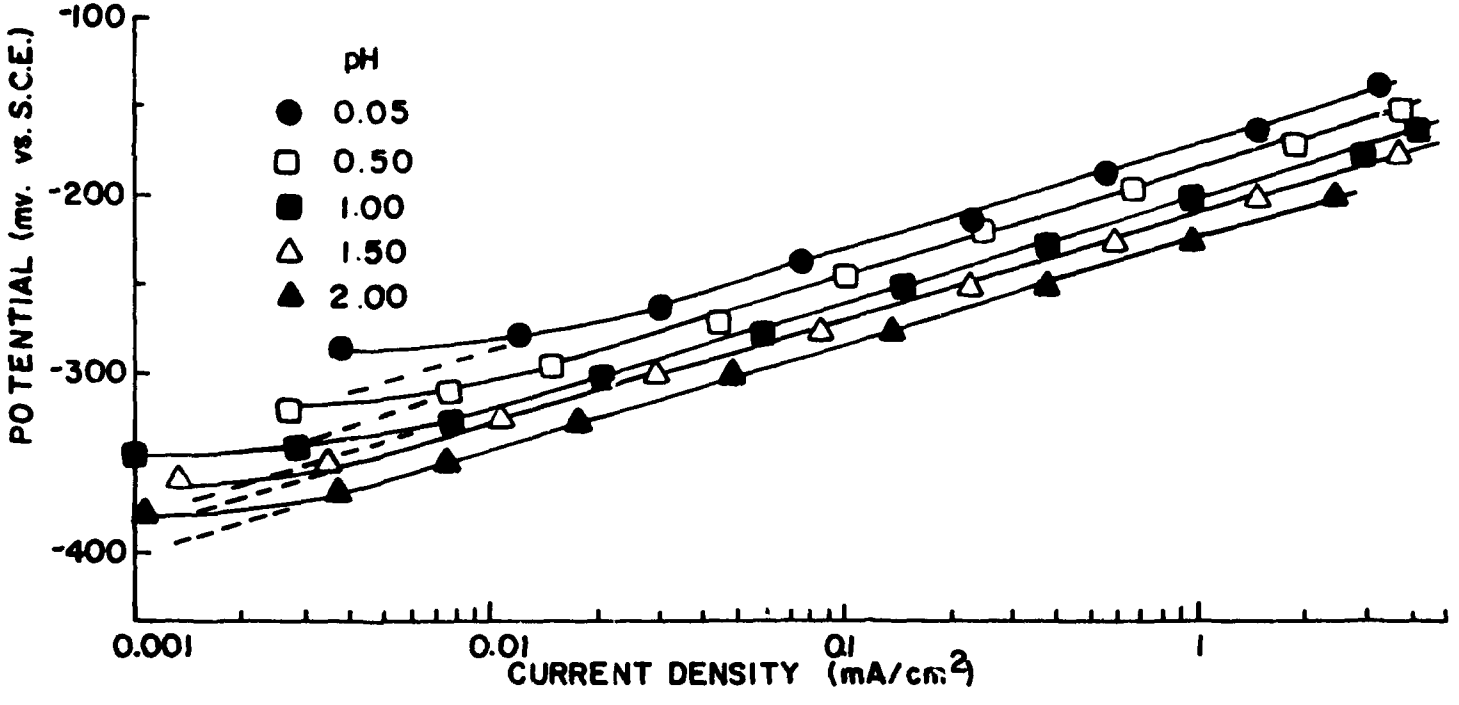

Figure 2. Anodic Dissolution of Nickel in x M HCl + (1-x) M NaCl Effect on pH.

c. Corrosion rates: A log i_{corr} vs log (H^+) plot of the corrosion currents given in Table 1 shows that:

$$\frac{\partial \log i_{corr}}{\partial \log (H^+)} = 0.53 \qquad (1c)$$

2. Cl^- Effect in 1M H^+ Solutions ($xHCl + (1-x)\ HClO_4$)

a. Corrosion potentials: The steady state corrosion potentials, which are presented in Table 2, were affected by variations in rotation rate up to 7000 rpm. φ_{corr} shifted to more active values as (Cl^-) increased from 0 to 1M and followed the relationship,

$$\frac{\partial \varphi_{corr}}{\partial \log (Cl^-)} \approx 0.016 \text{ V} \qquad (2a)$$

b. Polarization behavior: Anodic polarization of nickel, which was independent of the rotation rate up to 7000 rpm, is shown in Figure 3. The rate of nickel dissolution increases with increase in (Cl^-). An anodic Tafel slope,

$$\left(\frac{\partial \varphi}{\partial \log I}\right)_{(Cl^-)} = 0.075 \text{ V/dec} \qquad (2b)$$

was obtained for the mixed HCl-$HClO_4$ electrolytes in contrast to the 60 mv/dec obtained for 1M HCl. For (Cl^-) of 0.00 and 0.01M, a sweep rate of 2 mv/min was required to obtain a well-defined Tafel behavior. For (Cl^-) of 0.025 and 0.050M, the sweep rate could be increased to 5 mv/min, and for $(Cl^-) \geq 0.1$ M, 10 mv/min sweep rate was adequate to obtain Tafel behavior.

c. Corrosion rates: Chloride ions accelerated the nickel corrosion rate as shown in Table 2. The dependence of the corrosion current on Cl^- followed the relationship,

$$\frac{\partial \log i_{corr}}{\partial \log (Cl^-)} = +0.24 \qquad (2c)$$

3. H^+ Effect in 5M Cl^- Solutions

Concentrations of H^+ were varied from 0.1 to 5M at $(Cl^-) = 5$M. Table 3 shows the results of these studies.

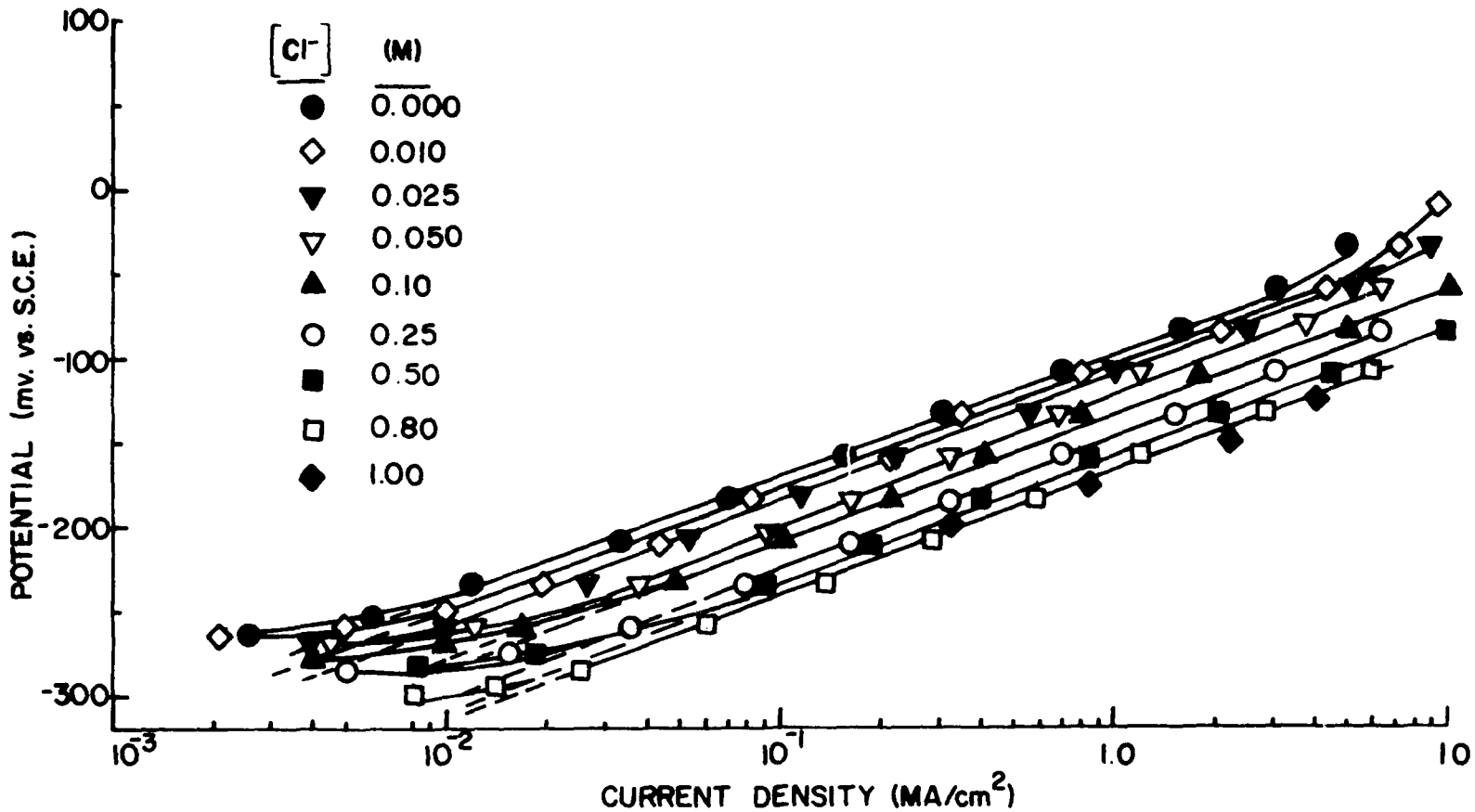

Figure 3. Anodic Dissolution of Nickel in xM HCl + (1-x) M $HClO_4$ Effect of Cl^-.

TABLE 3. Effect of H^+ on nickel dissolution in 5M Cl^- solutions.

Electrolyte	$[H^+]$ (M)	φ_{corr} (mv vs SCE)	Anodic Tafel Slope (mv vs dec)	i_{corr} ($\mu A/cm^2$)
0.1M HCl + 4.9M NaCl	0.10	-351± 3	65	10
0.17M HCl + 4.83M NaCl	0.17	-342± 3	65	11
0.32M HCl + 4.68M NaCl	0.32	-331± 2	65	16
0.5M HCl + 4.5M NaCl	0.50	-320± 1	65	18
0.75M HCl + 4.25M NaCl	0.75	-307± 4	65	20
1.0M HCl + 4.0M NaCl	2.0	-301± 6	65	24
2.0M HCl + 3.0M NaCl	2.0	-296± 5	65	45
3.0M HCl + 2.0M NaCl	3.0	-290± 6	65	59
4.0M HCl + 1.0M NaCl	4.0	-286± 2	65	88
5.0M HCl + 0.0M NaCl	5.0	-283± 8	65	115

TABLE 4. Effect of Cl^- on nickel dissolution in 5M H^+ solutions.

Electrolyte	$[Cl^-]$ (M)	φ_{corr} (mv vs SCE)	Anodic Tafel Slope (mv vs dec)	i_{corr} ($\mu A/cm^2$)
0.0M HCl + 5.0M $HClO_4$	0.000	-192± 2	80	19
0.01M HCl + 4.99M $HClO_4$	0.010	-195± 4	80	22
0.035M HCl + 4.965M $HClO_4$	0.035	-210± 5	80	27
0.1M HCl + 4.9M $HClO_4$	0.100	-220± 10	80	34
0.35M HCl + 4.65M $HClO_4$	0.35	-237± 4	80	48
1.0M HCl + 4.0M $HClO_4$	1.00	-253± 6	80	58
1.5M HCl + 3.5M $HClO_4$	1.50	-258± 3	62	68
2.5M HCl + 2.5M $HClO_4$	2.50	-266± 5	62	79
3.5M HCl + 1.5M $HClO_4$	3.50	-274± 3	62	90
5.0M HCl + 0.0M $HClO_4$	5.00	-283± 8	62	115

a. Corrosion potentials: As observed in the 5M H^+ electrolytes, the steady state values of φ_{corr} were reached almost immediately on immersion of the electrodes. Variations in the rotation speed had no effect on these corrosion potentials. An increase in H^+ concentration shifted φ_{corr} to more noble values. This shift is more pronounced at lower H^+ concentrations up to 1M, than at concentrations above 1M. The dependence of φ_{corr} on (H^+) was found to be

$$\frac{\partial \varphi_{corr}}{\partial \log (H^+)} = 0.049 \text{ V}; \qquad (H^+) < 1M \qquad (3a)$$

$$\frac{\partial \varphi_{corr}}{\partial \log (H^+)} = 0.025 \text{ V}; \qquad (H^+) \geq 1M \qquad (3a')$$

b. Polarization behavior: Anodic polarization was independent of the rotation rates but dependent on H^+ concentration as shown in Figure 4.

Anodic polarization curves were obtained at potential sweep rates of 10 mv/min and Tafel slopes,

$$\left(\frac{\partial \varphi}{\partial \log I}\right)_{(H^+)} = 0.065 \text{ V/dec} \qquad (3b)$$

were obtained for all H^+ concentrations. The effect of H^+ on anodic dissolution is different, depending on the concentration of H^+. For (H^+) between 1 to 5M, anodic dissolution of nickel was accelerated by H^+; between 0.1 to 1M, anodic dissolution decreased with increase in (H^+).

c. Corrosion rates: An increase in H^+ concentration increased i_{corr} as shown in Figure 5. The rate of increase is less for $(H^+) < 1M$ and greater for $(H^+) \geq 1M$.

$$\frac{\partial \log i_{corr}}{\partial \log (H^+)} = +0.4; \qquad (H^+) < 1M \qquad (3c)$$

and

$$\frac{\partial \log i_{corr}}{\partial \log (H^+)} = +0.9; \qquad (H^+) \geq 1M \qquad (3c')$$

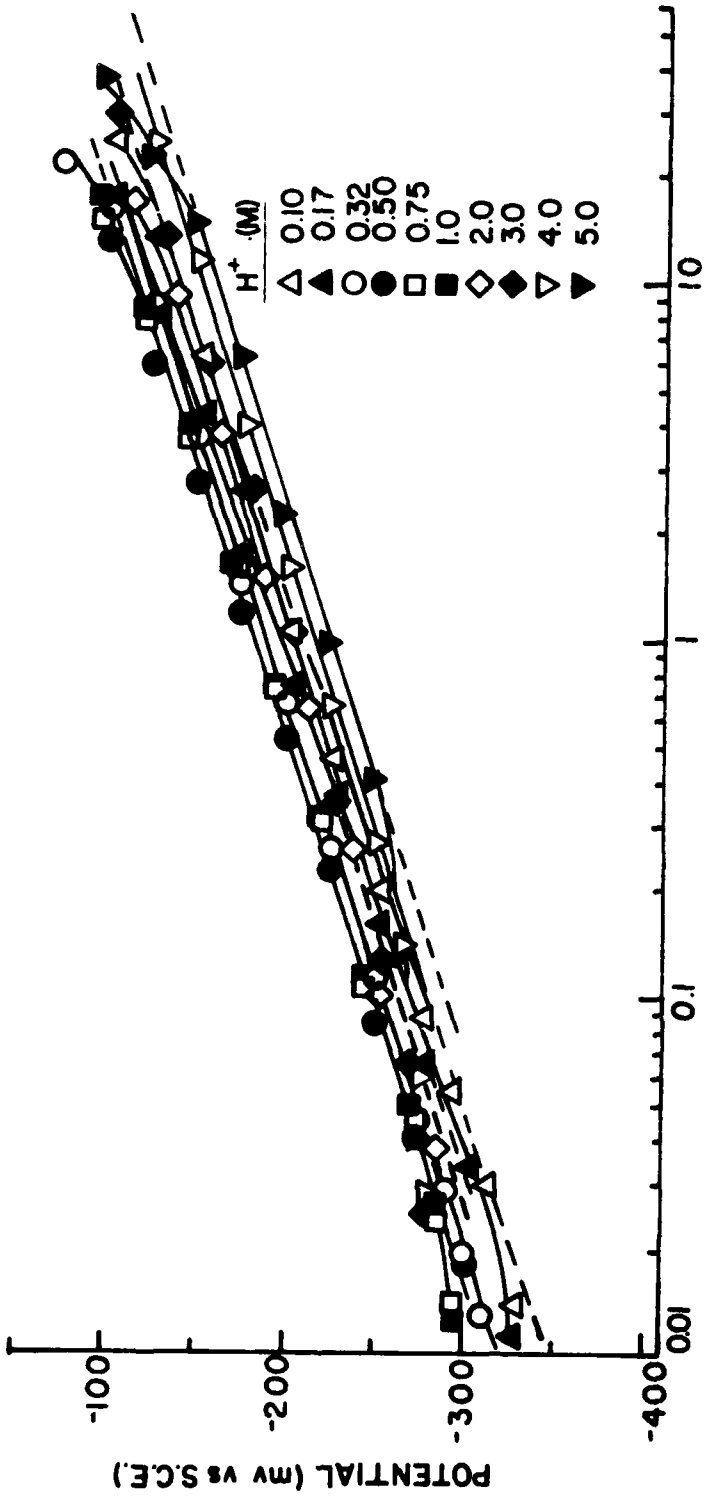

Figure 4. Anodic Dissolution of Nickel in xM HCl + (5-x) M NaCl. Effect of H^+.

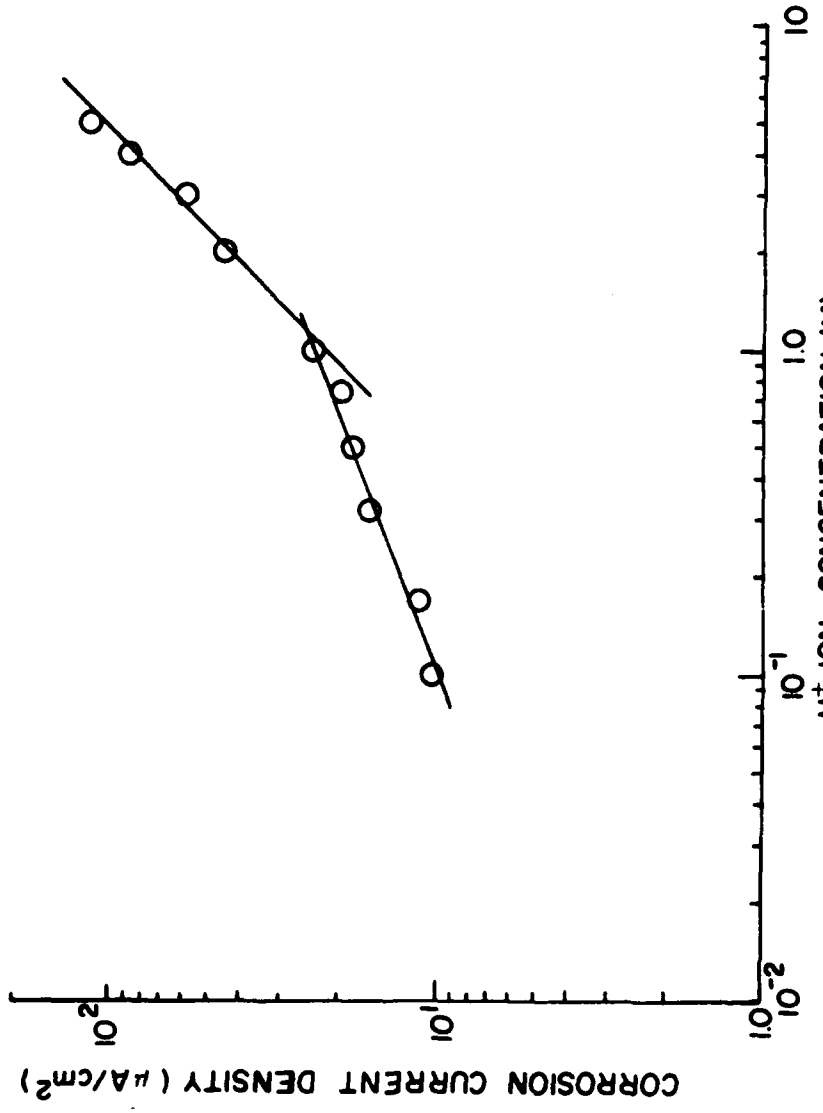

Figure 5. Corrosion Current of Nickel in xM HCl + (5-x) M NaCl. Effect of H^+.

4. Cl^- Effect in 5M H^+ Solutions ($xHCl + (5-x)\ HClO_4$)

a. Corrosion potential: The corrosion potentials reached steady state within 15 minutes after immersing the nickel electrodes in the electrolyte, which is more rapid than in the 1M electrolytes. These steady state φ_{corr} values, which are presented in Table 4, were unaffected by varying the rotation speeds. Increase in chloride ions shifted the φ_{corr} values in the active direction. However, the dependence of φ_{corr} on $(Cl^-) < 1.0M$ is different than at higher (Cl^-). These relationships are as follows,

$$\frac{\partial \log \varphi_{corr}}{\partial \log (Cl^-)} = -0.025\ V; \qquad (Cl^-) < 1.0M \qquad (4a)$$

$$= -0.048\ V; \qquad (Cl^-) \geq 1.0M \qquad (4a')$$

b. Polarization behavior: Figure 6 shows the anodic polarization curves which were independent of the rotation speed. Reproducible, well-defined Tafel behavior could be obtained at all sweep rates below 10 mv/min. It is shown that chloride ions accelerated the anodic dissolution of nickel. The anodic Tafel slopes were

$$\left(\frac{\partial \varphi}{\partial \log I}\right)_{(Cl^-)} = 0.080\ V/dec; \qquad (Cl^-) \leq 1M \qquad (4b)$$

$$\left(\frac{\partial \varphi}{\partial \log I}\right)_{(Cl^-)} = 0.062\ V/dec; \qquad 1 < (Cl^-) \leq 5M \qquad (4b')$$

c. Corrosion rates: Chloride ions accelerated the corrosion of nickel in the entire range of (Cl^-). Figure 7 shows a discontinuity in the corrosion current dependence on Cl^- between 0.35 - 1M Cl^-. Thus,

$$\frac{\partial \log i_{corr}}{\partial \log (Cl^-)} = +0.22; \qquad (Cl^-) < 0.35\ M \qquad (4c)$$

and

$$\frac{\partial \log i_{corr}}{\partial \log (Cl^-)} = +0.42; \qquad (Cl^-) \geq 1.0M \qquad (4c')$$

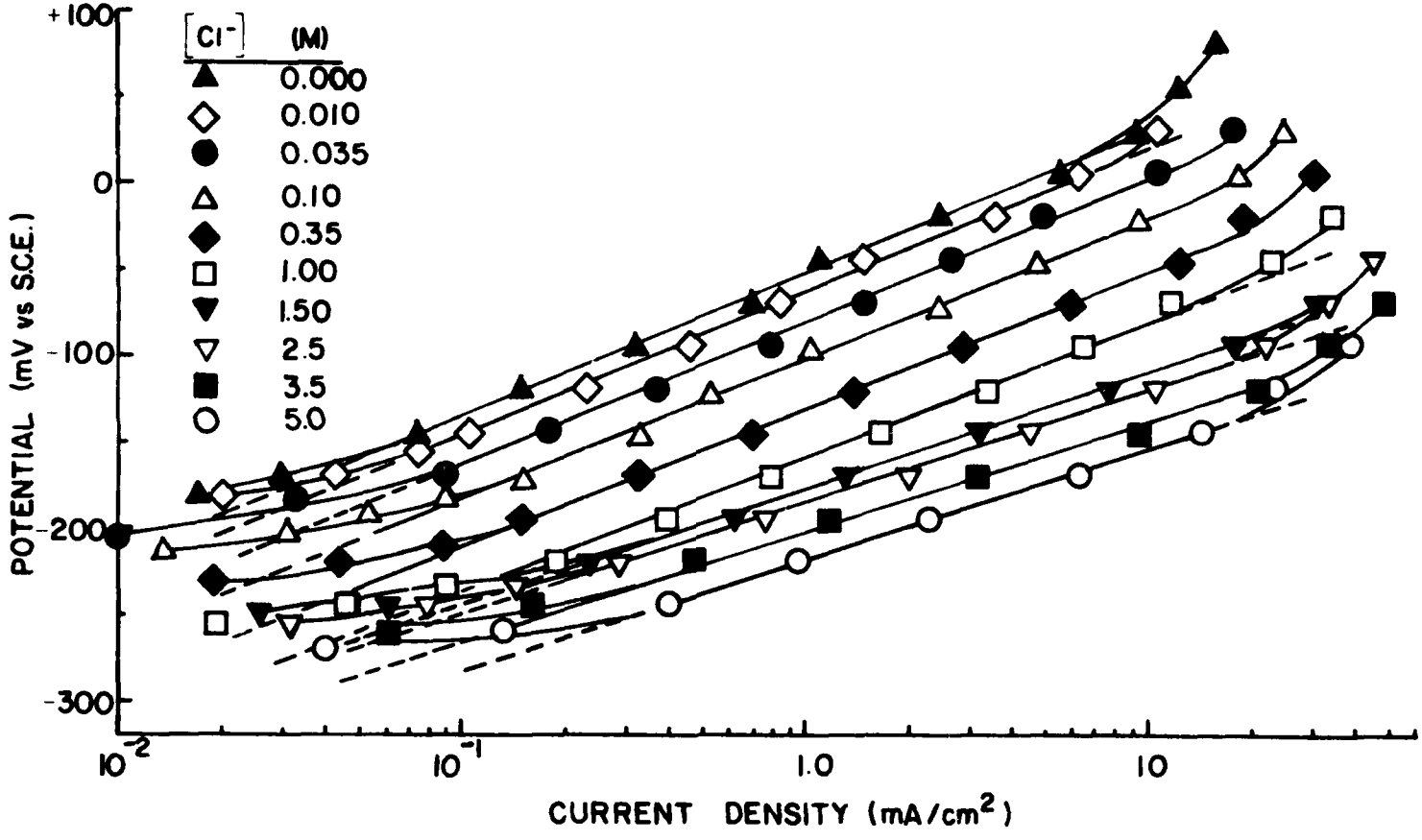

Figure 6. Anodic Dissolution of Nickel in xM HCl + (5-x) M $HClO_4$. Effect of Cl^-.

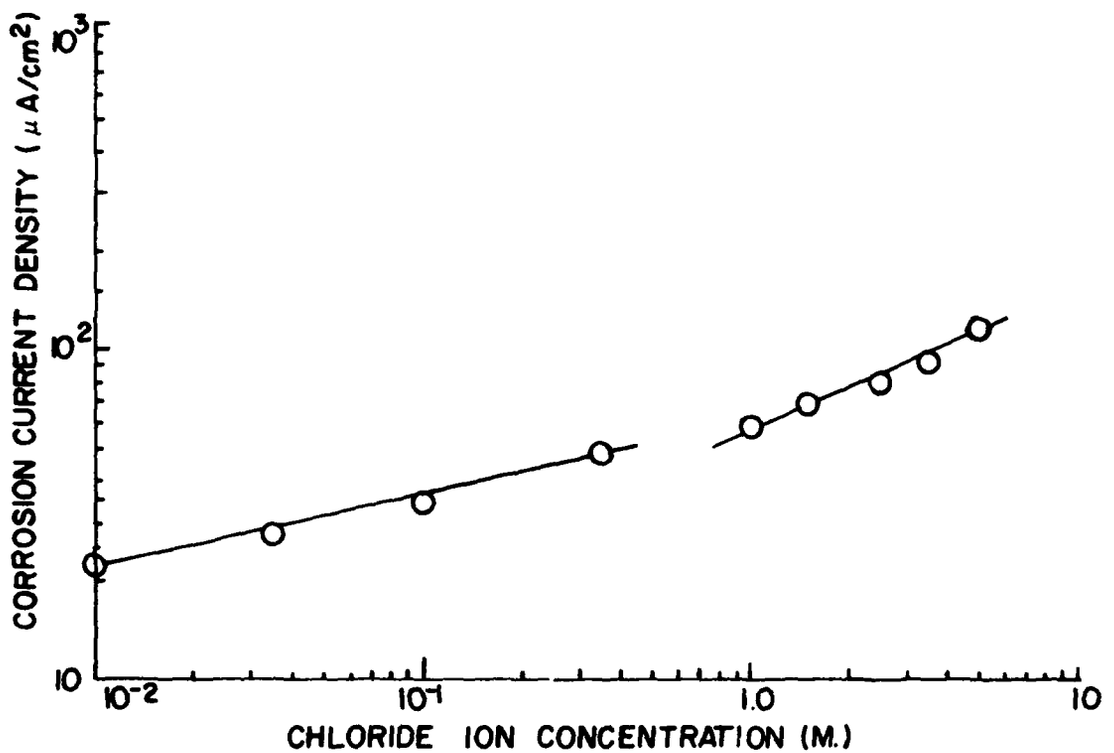

Figure 7. Corrosion Current of Nickel in xM HCl + (5-x) M $HClO_4$. Effect of Cl^-.

DISCUSSION

Anodic Dissolution of Nickel in 1M Ionic Strength Solutions

A direct measure of the dependence of nickel dissolution on H^+ or OH^- and Cl^- can be obtained by a reaction order plot such as Figure 8 which shows the dependence on pH. It is seen that nickel dissolution increases as (OH^-) increases or as (H^+) decreases. The slope of the line, which gives the reaction order for the anodic dissolution of nickel with respect to OH^-, is

$$\left(\frac{\partial \log i_a}{\partial \log (OH^-)}\right)_{\varphi} = 0.5 \qquad (5a)$$

or

$$\left(\frac{\partial \log i_a}{\partial \log (H^+)}\right)_{\varphi} = -0.5 \qquad (5b)$$

In the concentration range studied, Cl^- accelerated the anodic dissolution of nickel as shown in Figure 9 which gives the Cl^- reaction order as

$$\left(\frac{\partial \log i_a}{\partial \log (Cl^-)}\right)_{\varphi} = 0.5 \qquad (6)$$

Thus, Equations (5a) and (6) show that the rate of anodic dissolution of nickel in low H^+ concentration (<1M) and low Cl^- concentration (<1M) solutions can be described by the empirical expression:

$$i_{a,OH} = k'_{a,OH} (Cl^-)^{0.5} (OH^-)^{0.5} \exp\left(\frac{F\varphi}{RT}\right) \qquad (7)$$

The following mechanism is tentatively proposed to describe nickel dissolution in the 1M ionic strength solutions:

$$Ni + Cl^- + H_2O \underset{k_{-1}}{\overset{k_1}{\rightleftharpoons}} (NiClOH)_a^- + H^+ + e \qquad (8a)$$

$$(NiClOH)_a^- \xrightarrow{k_2} (NiClOH) + e \qquad (8b)$$

$$(NiClOH) + H^+ \underset{k_{-3}}{\overset{k_3}{\rightleftharpoons}} Ni^{++} + Cl^- + H_2O \qquad (8c)$$

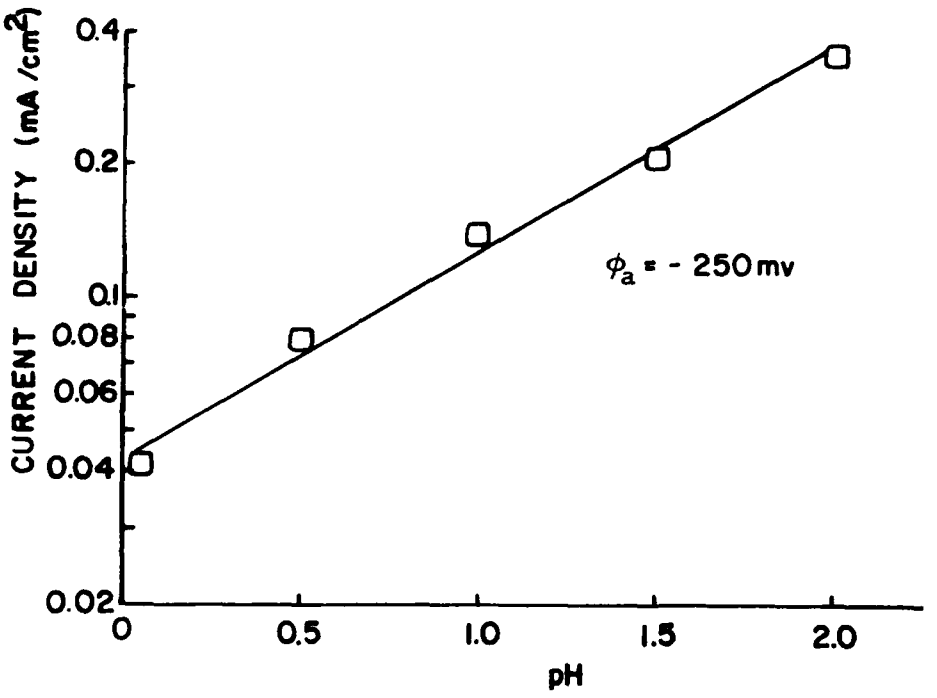

Figure 8. Reaction Order with respect to pH for Nickel Dissolution in xM HCl + (1-x) M NaCl.

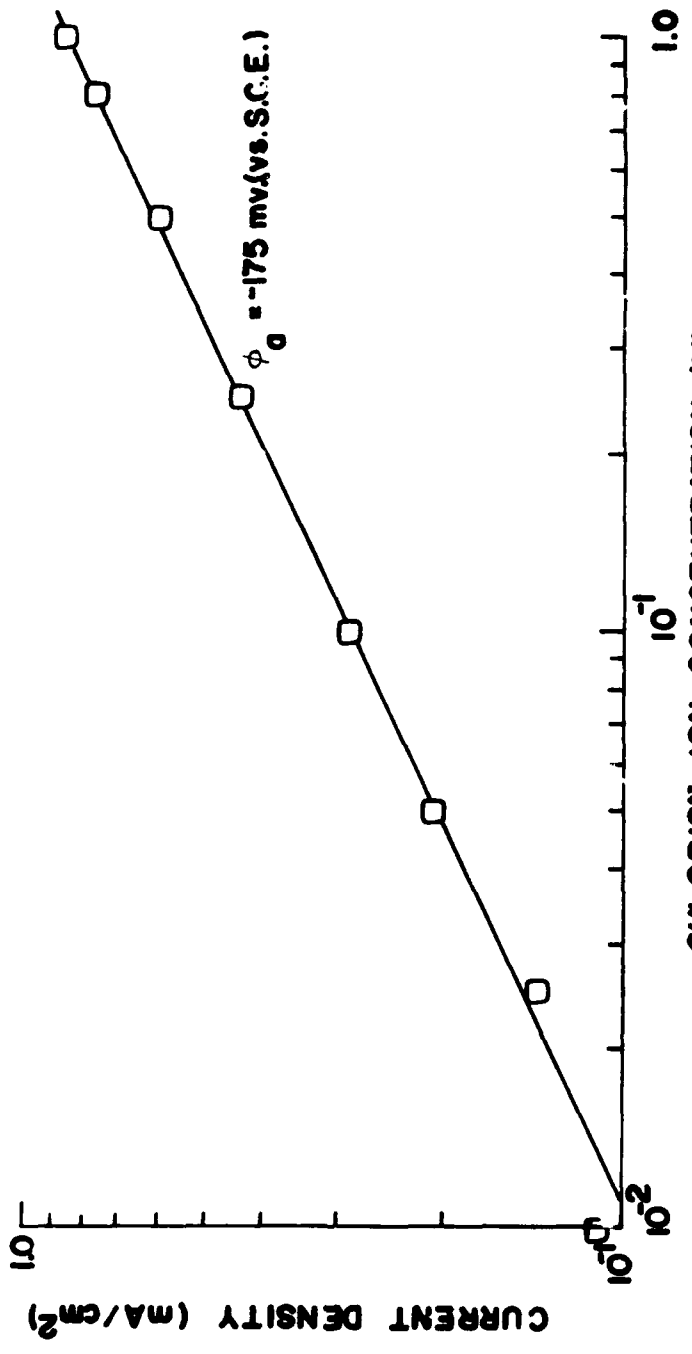

Figure 9. Reaction Order with respect to Cl^- for Nickel Dissolution in xM HCl + (1-x) M $HClO_4$.

If it is assumed that the surface coverage of $(NiClOH)^-_a$ is between 0.2 and 0.8, the Temkin adsorption isotherm can be utilized to determine $\theta_{(NiClOH)^-}$. Then, the free energy of adsorption of $(NiOHCl)^-$ can be expressed as a linear function of its surface coverage,

$$\Delta G'^{o}_{\theta} = \Delta G'^{o}_{o} - f' RT \theta \qquad (9)$$

where $\Delta G'^{o}_{o}$ is the free energy at the bare surface, R is the gas constant, T is the absolute temperature and f' is the Temkin adsorption parameter for $(NiClOH)^-_a$. If step (8b) is the rate determining step, step (8a) is at quasi-equilibrium and

$$\exp(f\theta) = \frac{k_1}{k_{-1}} (Cl^-)(OH^-) \exp\left(\frac{F\varphi}{RT}\right) \qquad (10)$$

Since

$$r_2 = k_2 \exp\left(\frac{\beta_2 F\varphi}{RT}\right) \exp(\gamma_2 f\theta) \qquad (11)$$

where β_2 and γ_2 are the charge transfer and adsorption symmetry factors. Equations (10) and (11) give

$$r_2 = k_2 (Cl^-)^{\gamma_2} (OH^-)^{\gamma_2} \exp \frac{(\beta_2 + \gamma_2) F\varphi}{RT} \qquad (12)$$

Thus, if $\beta_2 = 0.5$ and $\gamma_2 = 0.5$, the rate of anodic dissolution of nickel is

$$i_{a,OH} = k_{a,OH} (Cl^-)^{0.5} (OH^-)^{0.5} \exp\left(\frac{F\varphi}{RT}\right)$$

which is in accord with the experimental results as expressed by Equation (7). More details of the derivations of the above rate equation is given elsewhere, (2). The mechanism proposed for nickel dissolution is analogous to the mechanism proposed in Part II of this report for iron dissolution in low (H^+)- high (Cl^-) solutions.

Anodic Dissolution of Nickel in 5M Ionic Strength Solutions

The reaction order plot in Figure 10 shows that the pH dependence of nickel dissolution in this higher ionic strength solution is the same as in the lower ionic strength solutions for lower (H^+). That is,

$$\left(\frac{\partial \log i_a}{\partial \log (H^+)}\right)_{\varphi} = -0.5; \qquad (H^+) < 1M \tag{13}$$

On the other hand, at higher (H^+), nickel dissolution is accelerated by H^+ as shown in Figure 10. This reaction order plot shows that

$$\left(\frac{\partial \log i_a}{\partial \log (H^+)}\right)_{\varphi} = 0.6; \qquad 1 \leq (H^+) \leq 5M \tag{14}$$

Figure 11 shows the dependence of nickel dissolution on the mean activity of H^+, $[H^+]$,

$$\left(\frac{\partial \log i_a}{\partial \log [H^+]}\right)_{\varphi} = -0.5; \qquad [H^+] < 1M \tag{15}$$

and

$$\left(\frac{\partial \log i_a}{\partial \log [H^+]}\right)_{\varphi} = 0.6; \qquad 1 \leq [H^+] \leq 5M \tag{16}$$

The dependence of nickel dissolution on Cl^- at higher concentrations is different than at lower concentrations as shown in Figure 12. The dependence at lower (Cl^-) is the same as observed for nickel dissolution in 1M ionic strength solutions. That is,

$$\left(\frac{\partial \log i_a}{\partial \log (Cl^-)}\right)_{\varphi} = 0.5; \qquad (Cl^-) < 1M \tag{17}$$

However, at higher (Cl^-)

$$\left(\frac{\partial \log i_a}{\partial \log (Cl^-)}\right)_{\varphi} = 1.3; \qquad 1 \leq (Cl^-) \leq 5M \tag{18}$$

The experimental results show that for 5M ionic strength solutions at low (H^+) - low (Cl^-) the rate of nickel dissolution can be expressed as

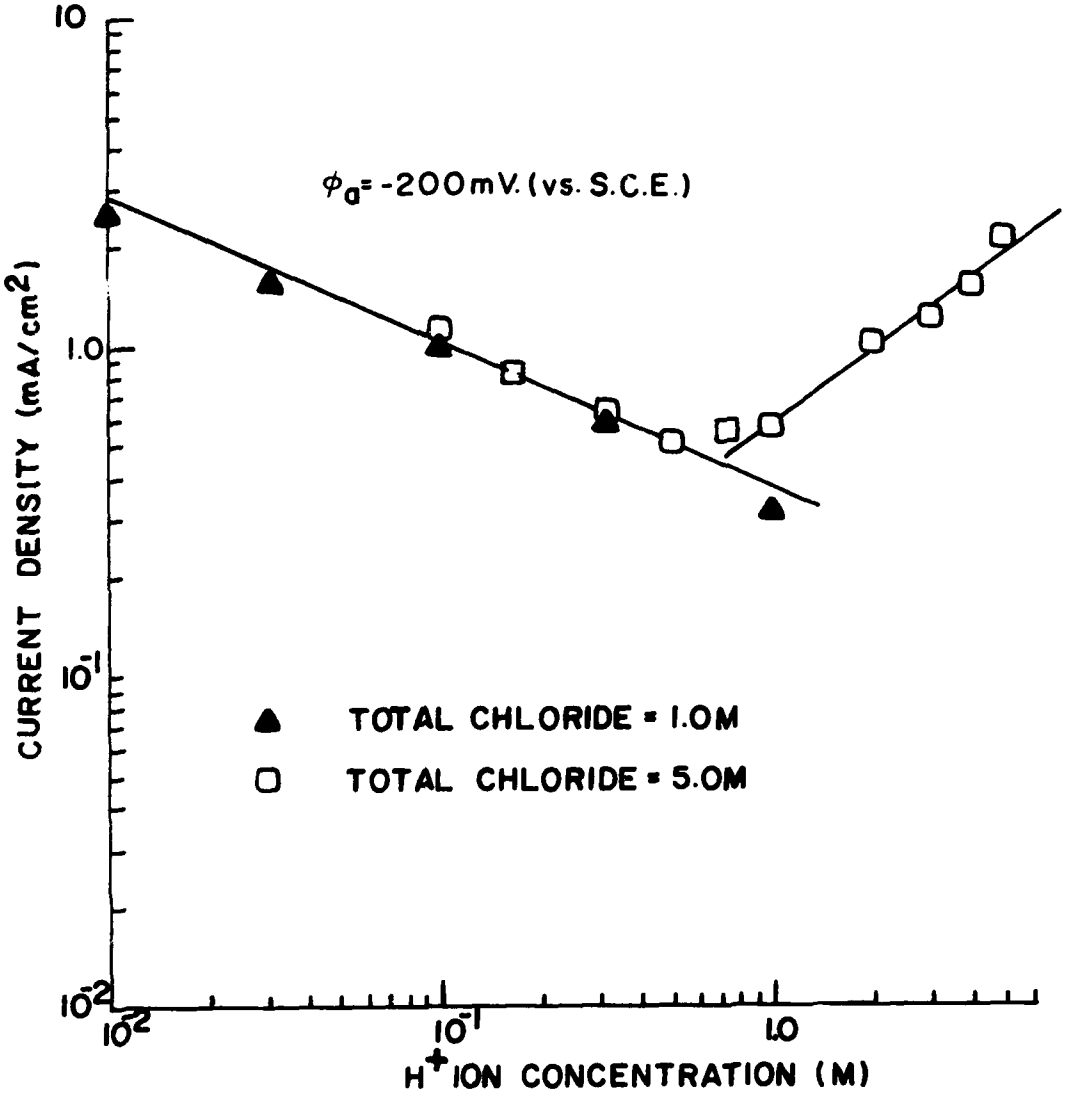

Figure 10. Reaction Order with respect to H^+ for Nickel Dissolution in xM HCl + (1-x)M NaCl and xM HCl + (5-x)M NaCl.

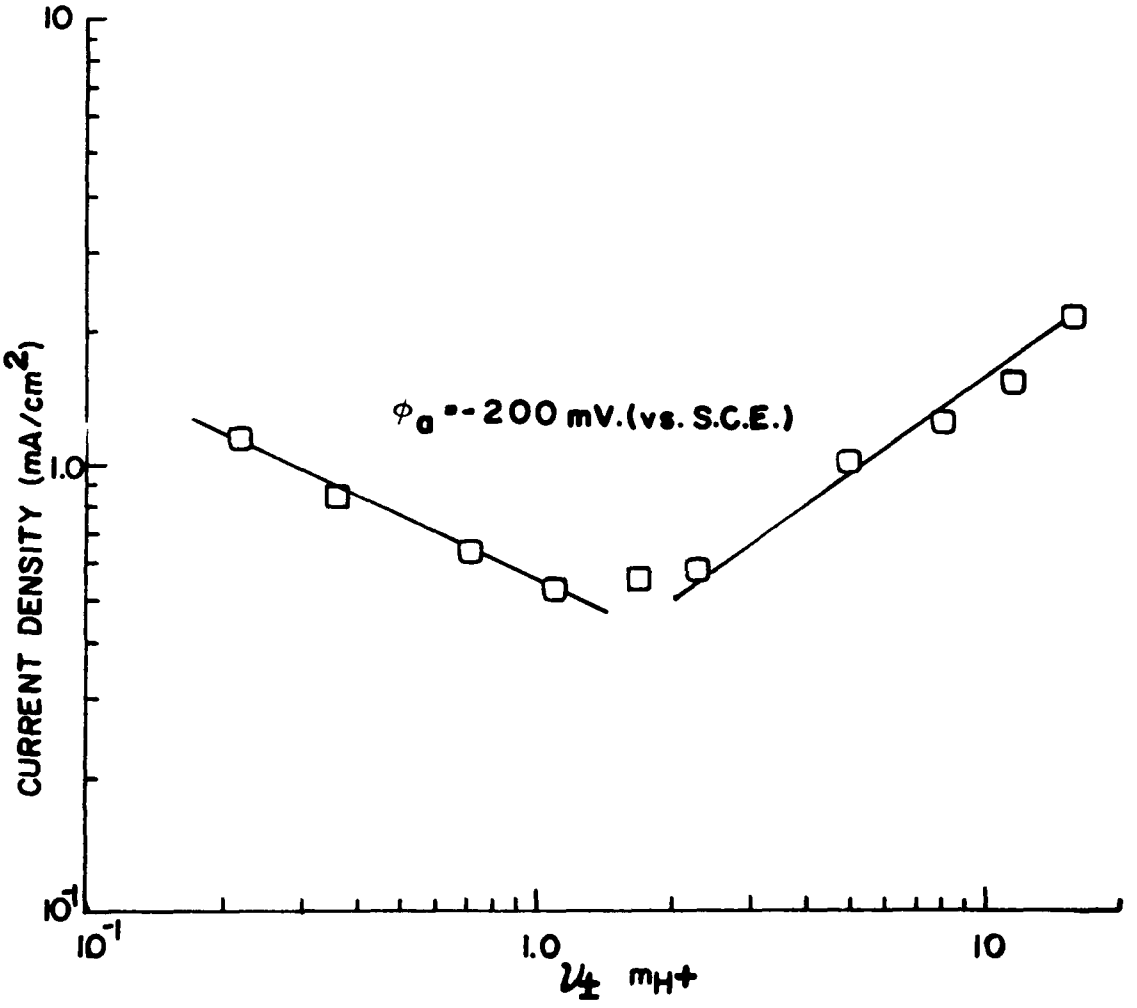

Figure 11. Reaction Order with respect to Activity of H^+ for Nickel Dissolution in xM HCl + (5-x) M NaCl.

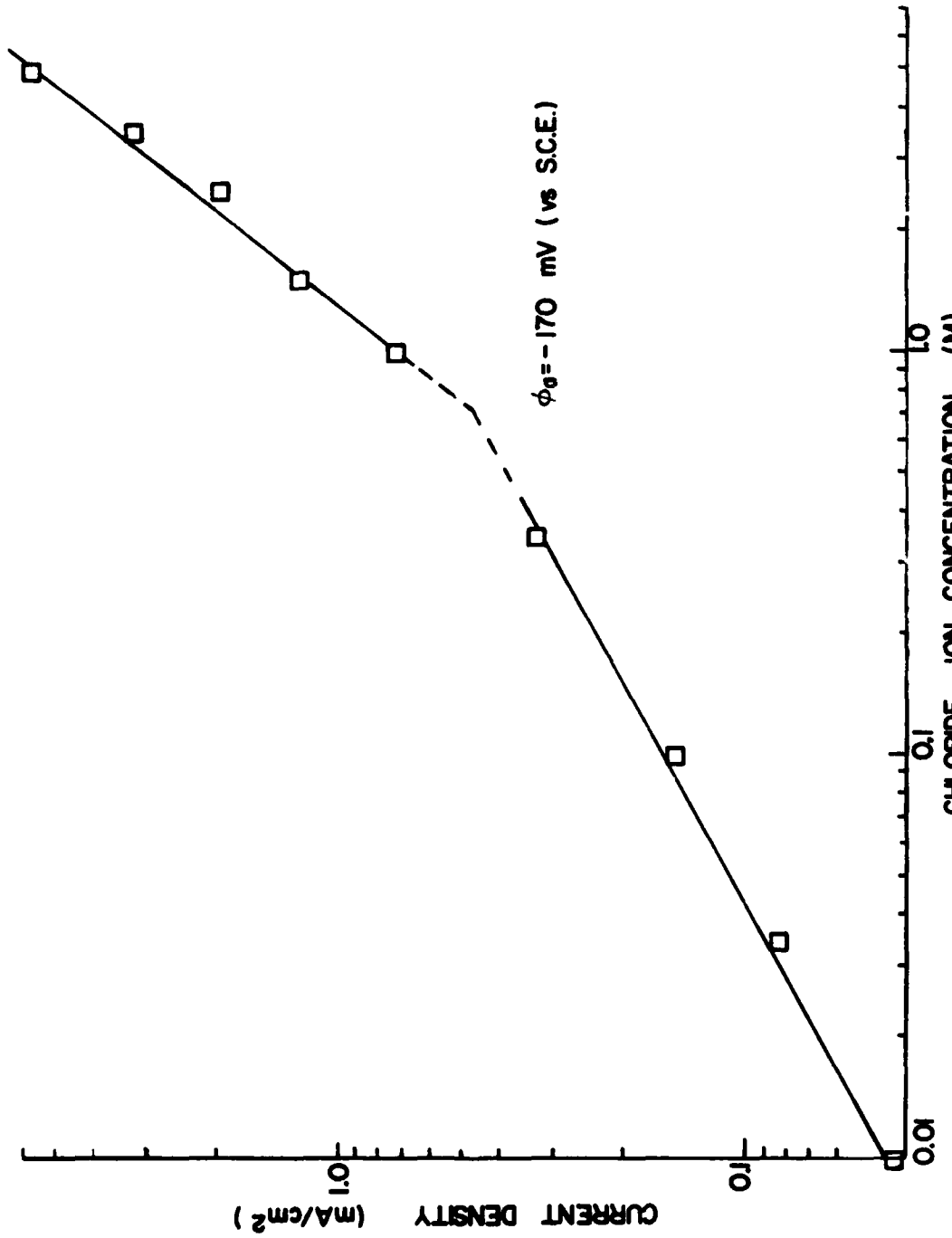

Figure 12. Reaction Order with respect to Cl^- for Nickel Dissolution in xM HCl + (5-x) M $HClO_4$.

$$i_{a,OH} = k_{a,OH}(OH^-)^{0.5}(Cl^-)^{0.5} \exp\left(\frac{F\varphi}{RT}\right); \qquad (H^+), (Cl^-) < 1M$$

On the other hand, for high (H^+)- high (Cl^-), the empirical rate of nickel dissolution is

$$i_{a,H} = k_{a,H}[H^+]^{0.6}(Cl^-)^{1.3}\exp\left(\frac{F\varphi}{RT}\right); \qquad 1 \leq [H^+] \leq 5M$$

$$1 \leq (Cl^-) \leq 5M \quad (19)$$

Nickel dissolution in the low (H^+)-low (Cl^-) 5M ionic strength solutions can be described by the mechanism proposed for nickel dissolution in the 1M ionic strength solutions. A tentative mechanism for nickel dissolution in the high (H^+)-high (Cl^-) solutions is proposed:

$$Ni + Cl^- + H^+ = (NiClH)_a^+ + e \quad (20a)$$

$$(NiClH)_a^+ \rightarrow NiCl_2 + H^+ + e \quad (20b)$$

$$NiCl_2 = Ni^{++} + 2\,Cl^- \quad (20c)$$

Equation (20b) is assumed to be the rate determining step, and the adsorbed intermediate $(NiClH)_a^+$ is assumed to follow Temkin adsorption behavior. Since Equation (20a) is at quasi-equilibrium,

$$\exp\left(\frac{f''\theta''}{RT}\right) = K_{(a)}(Cl^-)[H^+]\exp\left(\frac{F\varphi}{RT}\right) \quad (21)$$

where $K_{(a)}$ is the ratio of the rate constants of Equation (20a), f'' is the Temkin adsorption parameter for $(NiClH)_a^+$ and θ'' is the surface coverage of $(NiClH)_a^+$ The rate of Equation (20b) is

$$r_{(b)} = k_{(b)}(Cl^-)\exp\left(\frac{\beta_2 F\vartheta}{RT}\right)\exp\left(\frac{\gamma_2 f''\theta''}{RT}\right) \quad (22)$$

By substituting Equation (21) into (22)

$$r_{(b)} = k''_{(b)}(Cl^-)^{1+\gamma_2}[H^+]^{\gamma_2}\exp\left(\frac{(\beta_2+\gamma_2)F\varphi}{RT}\right) \quad (23)$$

If $\beta_2 = 0.5$ and $\gamma_2 = 0.5$, the rate of nickel dissolution is

$$i_{a,H} = k'_{a,H} (Cl^-)^{1.5} [H^+]^{0.5} \exp\left(\frac{F\varphi}{RT}\right) \qquad (24)$$

Equation (24) shows that the mechanism proposed in Equations (20a) to (20c) is consistent with the experimental results described by the empirical rate expression, Equation 19.

REFERENCES

1. Bengali, A.M., "Anodic Dissolution of Nickel in Acidic Chloride Media," Ph.D. dissertation, UCLA, March 1975.

2. Chin, R.J. and Ken Nobe, J. Electrochem. Soc., 119, 1457, 1972.

PART II

IRON DISSOLUTION IN DILUTE AND CONCENTRATED ACIDIC CHLORIDE SOLUTIONS

H. C. KUO AND KEN NOBE

ABSTRACT

The anodic dissolution of iron in acidic chloride solutions of constant ionic strengths of 1M and 4.5M has been investigated. Perchloric acid and sodium perchlorate were used as supporting electrolytes. The concentrations of H^+ and Cl^- were varied over a wide range to determine the effect of each ion separately on iron dissolution. In low H^+-high Cl^- concentrations, iron dissolution is accelerated by both Cl^- and OH^- at low polarization potentials and is accelerated by only OH^- at high polarization. The empirical rate equations have been determined as

$$i_a = K_a (Cl^-)^{0.4} (OH^-)^{0.6} \exp\left(\frac{3F\varphi}{4RT}\right); \qquad \text{at low polarization}$$

and

$$i_a = K'_a (OH^-)^{1.1} \exp\left(\frac{3F\varphi}{2RT}\right); \qquad \text{at high polarization.}$$

On the other hand, iron dissolution in high H^+- high Cl^- concentrations is accelerated by H^+ rather than by OH^- as in low H^+-high Cl^- solutions. Furthermore, iron dissolution in these concentrated acidic chloride solutions is more strongly accelerated by Cl^-. The empirical rate of iron dissolution has been determined as

$$i_a = k_a [H^+]^{0.9} [Cl^-]^{1.1} \exp\left(\frac{F\varphi}{2RT}\right)$$

for high H^+ - high Cl^- solutions.

For high H^+ - low Cl^- concentrations, iron dissolution is inhibited by chloride ions and the empirical rate of anodic dissolution has been determined as

$$i_a = k''_a (OH^-) (Cl^-)^{-\delta} \exp\left(\frac{(3/2 - \delta) F\varphi}{RT}\right)$$

where δ changes from 0 to 1 with increasing Cl^-.

INTRODUCTION

There have been numerous investigations of the electrochemical behavior of iron and iron-base alloys in chloride media due to its practical importance in corrosion. It is well known (1,2) that the presence of chloride ions in the solution can affect the corrosion rate and induce pitting and crevice corrosion. A thorough understanding of the role of chloride ions in the anodic dissolution of iron is important for developing methods o prevent or minimize this insidious type of localized corrosion.

Although there have been numerous studies the actual details of how chloride ions affect iron corrosion is still not understood. Recently it has been suggested that adsorbed chloride ions actually participate directly in electrodissolution of iron (3-7). Different mechanisms to account for this result have been proposed.

Few of the previous investigations have examined more concentrated chloride solutions than 1M. In order to simulate the environment for iron corrosion within pits and crevices, recent investigations have focussed more attention to iron dissolution in concentrated chloride solutions.

Recent work (8,9) has shown that the anodic dissolution behavior of iron in concentrated chloride solutions is different than that in solutions of low chloride concentrations. Since the results of different research workers are not in agreement, it seems appropriate to investigate in more detail iron dissolution in solutions with chloride concentrations varying over a wide range.

This report presents results of a study of the anodic dissolution of iron rotating disk electrodes in acidic solutions in which the hydrogen ion and chloride ion concentrations are varied over a wide range with the ionic strength maintained at 4.5M.

EXPERIMENTAL

The rotating disk electrode system and the electrochemical cell were similar to that shown in Figure 1 of the previous chapter. The assembly consisted basically of a firmly mounted vertical quill which held the working electrode via a collet chuck. The quill was driven by a 1/8 H.P. Bodine D.C. motor through a belt and pulley system. The speed of the motor was controlled and maintained to within 0.5% by a Minarik SL-32 variable speed controller.

The test electrodes used in this investigation were made from a 1.27 cm (0.5 in.) diameter rod of Ferrovac E iron. The rod was first turned down and polished on a lathe to a diameter of 1.257 cm (0.495 in.). It was then cut into 1.27 cm. lengths using an abrasive wheel of Al_2O_3. During the cutting process, water was used to cool the electrode. Both faces of the electrodes were polished with waterproof alumina paper of various grit (#240 #400 and # 600). After polishing, the electrodes were washed and rinsed in distilled water, degreased with hot benzene in a Soxhlet column for four hours and then annealed under vacuum ($< 10^{-4}$ mm Hg) at 700°C for one hour and cooled down slowly to room temperature. The exposed area of the finished disk electrode was 1.242 sq. cm.

The reference electrode was a saturated calomel electrode (S.C.E.). All potentials reported in this study were referred to this electrode. The reference electrode was housed in a small glass reservoir and connected to the Luggin capillary through a glass tube.

In those experiments in which perchlorate ions were present in the electrolyte, a fiber junction salt bridge (double junction) was inserted between the saturated calomel electrode and working solution to preclude precipitation of potassium perchlorate within the fiber junction of the calomel electrode. This bridge was filled with 4.2 M NaCl solution.

A dual function Princeton Applied Research potentiostat/galvanostat (Model 173) with a current-voltage converter plug-in (P.A.R. Model 176) was used to control the potential between the test and reference electrode (potentiostat mode) or to supply constant current through the electrochemical cell (galvanostat mode). The potentiostat/galvanostat was built with two setting dials. The applied

potential or current could be switched electronically from one setting to another with 1 μ s. The switch could be triggered manually or by external triggering input from a function generator. In the potentiostatic mode, the potential difference between the working electrode and the reference electrode could be accurately and independently selected on the two setting dials with an accuracy of 1 mv between $\pm$ 5 volts.

The potential of the test electrode was measured with a Keithley electrometer (Model 602B). The current through the cell was measured either by the built in panel meter on the potentiostat/galvanostat or by a Simpson ammeter (Model 269) connected to the circuit.

A dual channel Moseley strip chart recorder (Model 1700A) was used to monitor the potential and current. An Exact function generator (Model 255) was connected to the potentiostat in order to supply the linear potential ramp or sweep during potentiodynamic polarization or the triggering pulse to switch the applied potential/current from one setting to another during polarization.

A Moseley x-y recorder (Model 7035A) was used to record the potential from the electrometer output and the current from the current-voltage output during potential sweep polarization. In the pulse polarization or transient study the current or potential transients were recorded on a Tektronix storage oscilloscope (Type 564).

All electrolytes were prepared from deionized water which was subsequently distilled and Analytical Reagent Grade Chemicals. The electrolyte was continually deaerated with prepurified grade nitrogen gas which was first passed through a heated (900^{o}F) copper column to remove the residual oxygen. The electrode was immersed in the electrolyte about twelve hours after the deaeration was started. Before immersion the electrode was activated in 5N HCl solution for 20 minutes, followed by thorough rinsing in a stream of deionized-distilled water. The potential of the working electrode was continuously monitored and recorded after immersion in the electrolyte. The rest (corrosion) potential usually achieved steady state within two hours. Polarization was started after about three hours immersion. In all of the polarization experiments, the rotation speed was fixed at 1000 rpm; however, a few experiments were performed by varying the rotation

speed to check for mass transfer effects.

The pH effect was studied in 4.5M HCl-NaCl solutions. The chloride effects were studied in the following solutions:

i) Solutions of pH = 1.05 ± 0.05 - 4.5M $NaCl$-$NaClO_4$ - $HClO_4$ electrolytes.

ii) 4.5M HCl -- $HClO_4$ solutions.

In both series, the concentration of chloride ions was varied from 0 to 4.5M.

RESULTS

All the polarization data presented in this report have been corrected for the IR drops. All potential values include corrections for the liquid junction potentials.

A. Effect of Hydrogen Ions on the Anodic Dissolution of Iron in 4.5 M Chloride Solutions (xM NaCl + yM HCl solutions with x + y = 4.5M).

1. Corrosion potentials

In this series, the corrosion potential reached steady state within two hours after immersion and was found to be independent of rotation rate. As shown in Table 1, φ_{corr} shifted to more noble potentials with increasing hydrogen ion concentration. For positive pH values, $\frac{\partial \varphi_{corr}}{\partial pH} = -51$ mv/pH. For negative pH values $H^+ > 1M$, $\frac{\partial \varphi_{corr}}{\partial \log (H^+)} = 35$ mv/dec.

2. Polarization behavior

Figure 1 shows the effect of pH on the steady state potentiostatic anodic polarization of iron in NaCl + HCl solutions with $(H^+) \leq 0.1$ M. Two Tafel regions were observed. At low polarization, a 78 mv/dec anodic Tafel slope was obtained. At high polarization anodic Tafel slopes were 40 mv/dec. The dissolution rate increased with increase in pH. The transition potential and corresponding current, determined at the intersection of the extrapolations of the two Tafel lines, depended on pH. These values are listed below:

TABLE 1. Effect of pH or H^+ on iron dissolution in 4.5M Cl^- solutions.

Electrolyte	pH	φ_{corr} (mv vs SCE)	Anodic Tafel Slope (mv/dec)	i_{corr} (ma/cm^2)
4.5M NaCl	4.25	-739± 5	85± 5	0.023
4.5M NaCl	2.65	-635± 7	82± 3	0.035
4.5M NaCl	2.00	-600± 5	72± 5	0.032
4.5M NaCl	1.22	-565± 10	78± 5	0.045
4.45M NaCl + 0.05M HCl	0.50	-515± 7	82± 2	0.077
4.45M NaCl + 0.1M HCl	0.24	-500± 5	80± 5	0.085
4.0M NaCl + 0.5M HCl		-430± 5	79± 5	0.275
3.5M NaCl + 1M HCl		-425± 8	110± 8	1.00
2.5M NaCl + 2M HCl		-395± 4	108± 5	3.10
1.5M NaCl + 3M HCl		-391± 5	110± 4	4.35
4.5M HCl		-397± 4	110± 5	6.95

TABLE 2. Effect of Cl^- on iron dissolution in pH = 1 solutions.

Electrolyte	pH	φ_{corr} (mv.vs.SCE)	Anodic Tafel Slopes (mv/dec)	i_{corr} (ma/cm^2)
4.49M $NaClO_4$ + 0.01M $HClO_4$ ($[Cl^-] < 10^{-4}$M)	1.09	-498± 2	40± 3	0.500
4.49M $NaClO_4$ + 0.01M $HClO_4$ + 0.001M NaCl	1.09	-501± 3	41± 3	0.093
4.49M $NaClO_4$ + 0.01M $HClO_4$ + 0.005M NaCl	1.09	-514± 4	47± 5	0.054
4.48M $NaClO_4$ + 0.01M $HClO_4$ + 0.01M NaCl	1.07	-516± 8	75± 5	0.030
4.47M $NaClO_4$ + 0.01M $HClO_4$ + 0.02M NaCl	1.07	-518± 5	80± 5	0.021
4.44M $NaClO_4$ + 0.01M $HClO_4$ + 0.05M NaCl	1.07	-523± 4	79± 5	0.021
4.39M $NaClO_4$ + 0.01M $HClO_4$ + 0.1M NaCl	1.07	-530± 7	76± 6	0.021
4.29M $NaClO_4$ + 0.01M $HClO_4$ + 0.2M NaCl	1.06	-533± 6	77± 3	0.019
3.99M $NaClO_4$ + 0.01M $HClO_4$ + 0.5M NaCl	1.05	-535± 6	75± 5	0.021
3.49M $NaClO_4$ + 0.01M $HClO_4$ + 1M NaCl	1.05	-547± 8	76± 4	0.023
2.49M $NaClO_4$ + 0.01M $HClO_4$ + 2M NaCl	1.04	-564± 8	75± 4	0.023
0.49M $NaClO_4$ + 0.01M $HClO_4$ + 4M NaCl	1.05	-573± 8	79± 5	0.027

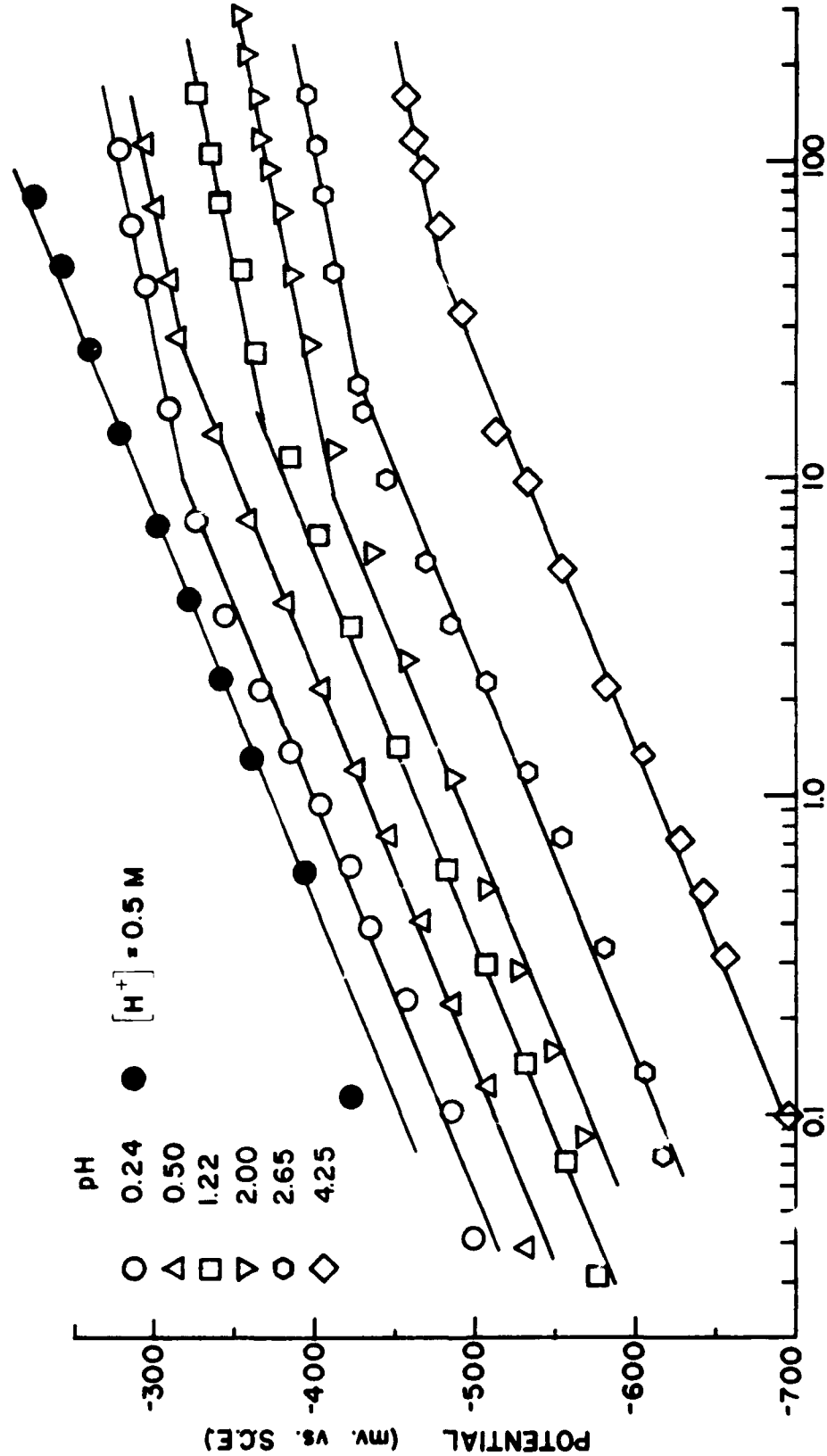

Figure 1. Anodic Dissolution of Iron in 4.5M NaCl-HCl Solutions; $(H^+) \leq 0.5M$

pH	Transition Potential (φ_t) (mv vs S.C.E.)	Transition Current (i_t) (ma/cm^2)
4.25	-480	45
2.65	-420	23
2.00	-405	18
1.22	-376	16
0.50	-337	15
0.24	-320	10

Plots of φ_t and i_t vs pH give $\frac{\partial \varphi_t}{\partial\ pH} \approx -38$ mv/pH and $\frac{\partial \log i_t}{\partial\ pH} = 0.16$.

Figure 2 shows the anodic polarization of iron in solutions with $(H^+) \geq 0.5M$. In 0.5M HCl + 4.0M NaCl solution, an anodic Tafel slope of 79 mv/dec was obtained in accord with the value obtained at lower H^+ concentrations. However, for $(H^+) \geq 1M$, the Tafel slope changed to 110 mv/dec, and the dissolution rate increased with the increase in (H^+) in contrast to the result obtained in solutions at lower (H^+).

3. Corrosion rates

The corrosion currents are presented in Table 1. The corrosion current did not vary appreciably at pH > 0, but changed greatly in highly acidic solutions, $(H^+) \geq 1$ M, $\frac{\partial \log i_{corr}}{\partial \log (H^+)} \approx 1.3$.

B. Effect of Chloride Ions on the Anodic Dissolution of Iron in Solutions of 4.5 Total Molarity Containing 0.01 M H^+ (xM NaCl + yM $NaClO_4$ + 0.01M $HClO_4$ solutions with x + y = 4.49, pH = 1.07 ± 0.05).

1. Corrosion potentials

The observed steady state corrosion potentials were independent of the rotation rate and are listed in Table 2. For (Cl^-) in the range 10^{-4} - 0.2M, $\frac{\partial \varphi_{corr}}{\partial \log (Cl^-)} \approx -10$ mv/dec. For $(Cl^-) > 0.2M$, $\frac{\partial \varphi_{corr}}{\partial \log (Cl^-)} \approx -32$ mv/dec.

2. Polarization behavior

Anodic potentiostatic polarization in this series of solutions is shown in Figures 3-5. Some steady state galvanostatic polarization results in selected solutions are also shown in Figure 3. In solutions with $(Cl^-) > 0.001M$, an anodic Tafel slope of 40 mv/dec was observed. The same results as potentiostatic polarization were obtained with galvanostatic polarization (Figure 3). With increasing (Cl^-) to 0.02M, the anodic Tafel slope increased

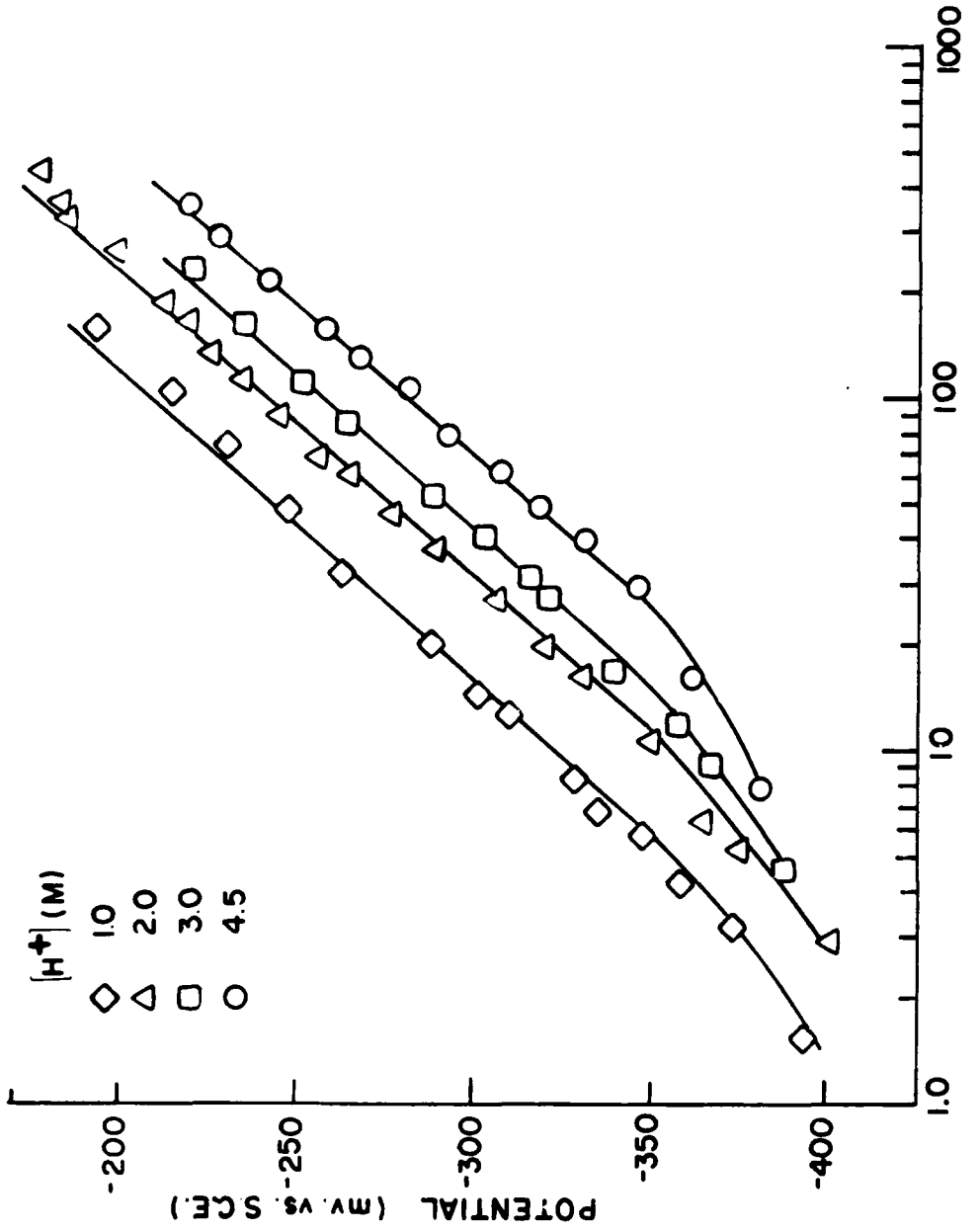

Figure 2. Anodic Dissolution of Iron in 4.5M NaCl-HCl Solutions; $(H^+) \geq 0.5M$.

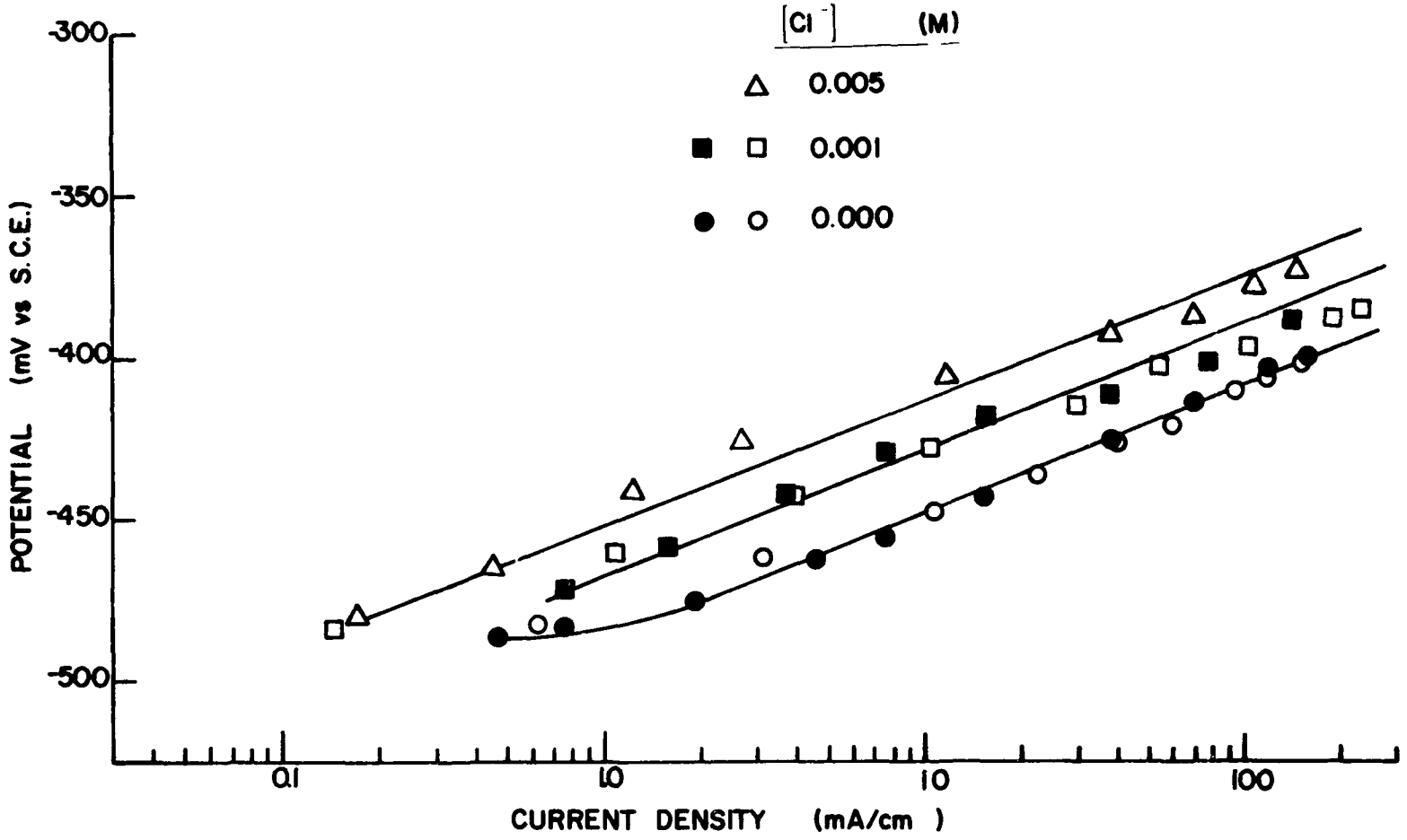

Figure 3. Anodic Dissolution of Iron in xM NaCl + yM $NaClO_4$ + 0.01M $HClO_4$ Solutions; x + y = 4.49, $(Cl^-) \leq 0.005M$.

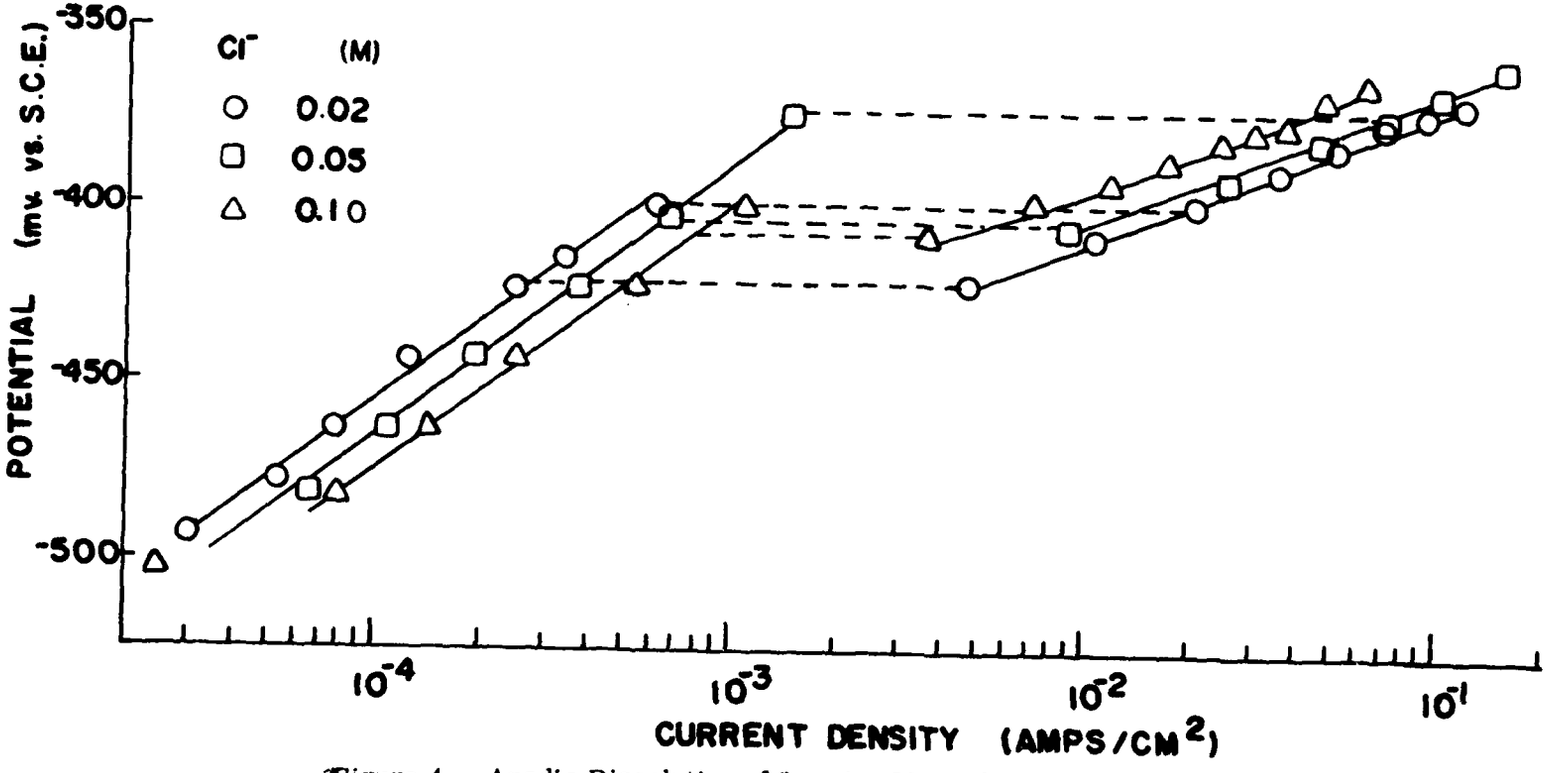

Figure 4. Anodic Dissolution of Iron in xM NaCl + yM $NaClO_4$ + 0.01M $HClO_4$ Solutions; x + y = 4.43, 0.02M $\leq (Cl^-) \leq$ 0.1 M.

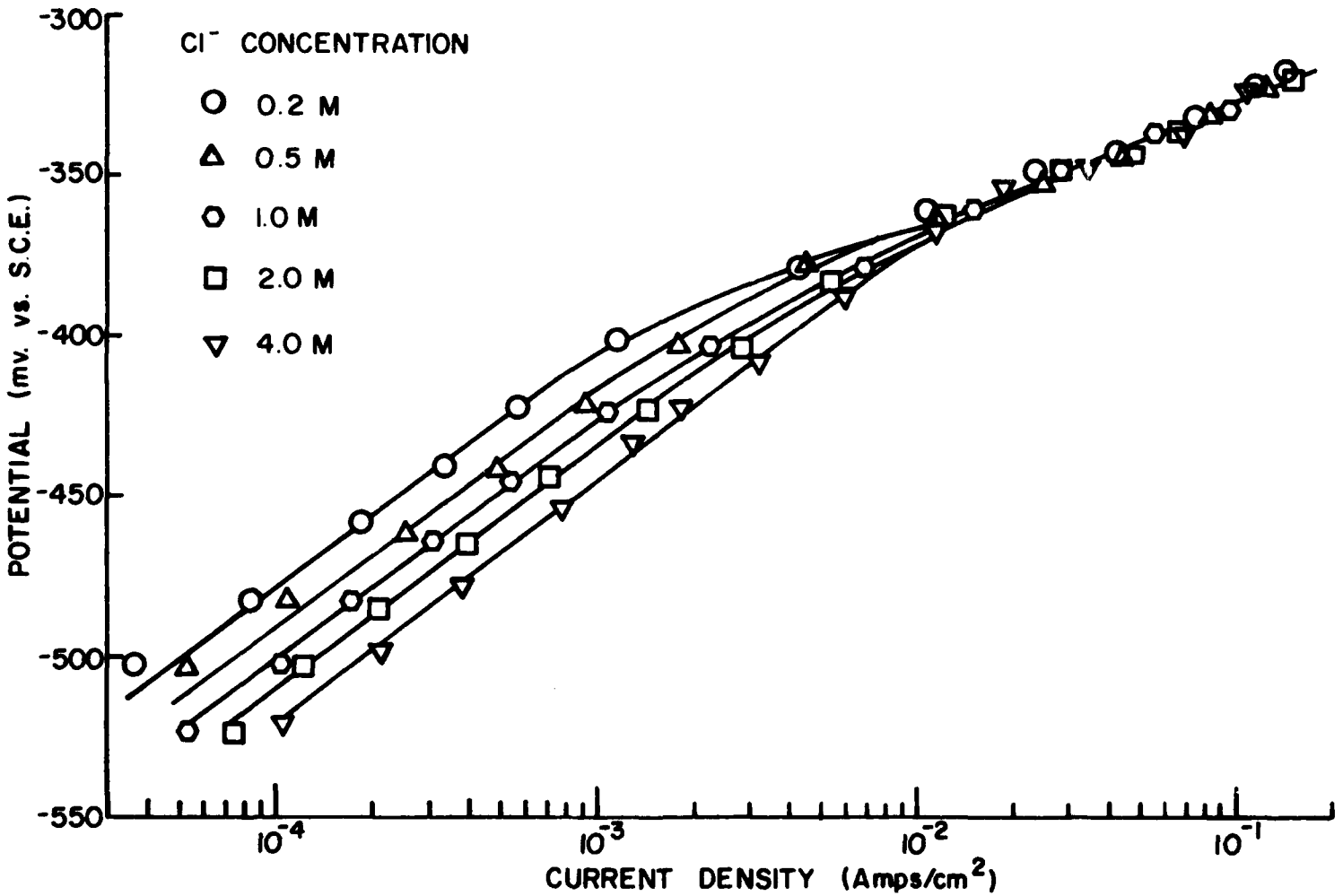

Figure 5. Anodic Dissolution of Iron in xM $NaCl$ + yM $NaClO_4$ + 0.01M $HClO_4$ Solutions; x + y = 4.49, 0.2M $\leq$ (Cl^-) $\leq$ 4M.

from 40 mv/dec to 75 mv/dec and Cl^- was observed to inhibit iron dissolution (Figure 3).

In solutions with (Cl^-) from 0.02 to 0.1 M (Figure 4), potentiostatic anodic polarizations initially exhibited 77 $\pm$ 7 mv/dec Tafel slopes. When the applied potential increased to more noble values than - 425 mv vs. S. C. E., the current transient initially exhibited a pseudo-steady state value (minimum), but it then increased gradually to a final steady state value. Figure 6 shows typical current transients in 0.01M chloride solutions at different potentials. The duration of the first pseudo-steady state current decreased rapidly with the increase in the applied anodic potential. The rate of increase of the current transient from the initial pseudo-steady state to the final steady state increased rapidly with increasing applied anodic potential. When the applied potential was higher than -370 mv, the final steady state current was reached within a few milliseconds. A plot of the final steady state current densities vs. potential at high polarization showed a Tafel slope of 40 mv/dec (Figure 4). As shown, chloride ions inhibited iron dissolution in the 40 mv/dec Tafel slope region, but at low polarization, the 77 mv/dec Tafel slope region Cl^- had an acceleration effect. In solutions with (Cl^-) > 0.1 M (Figure 5), potentiostatic polarization showed 77 mv/dec Tafel slopes at low polarization and 40 mv/dec at high polarization, similar to the results for (Cl^-) from 0.01 - 0.1M. However, the transition between the two Tafel regions was not as complicated as that shown in Figure 4. In the 77 mv/dec Tafel region the rate of iron dissolution was accelerated by Cl^-, but in the 40 mv/dec Tafel region no effect of chloride ions was observed.

3. Corrosion rates

Corrosion currents are presented in Table 2. It was observed that the corrosion current decreased rapidly with increasing chloride concentration in solutions in which (Cl^-) < 0.01 M, was unchanged in solutions with (Cl^-) between 0.01M to 0.2M, and then increased slightly with increase in chloride concentration in solutions in which (Cl^-) > 0.2M.

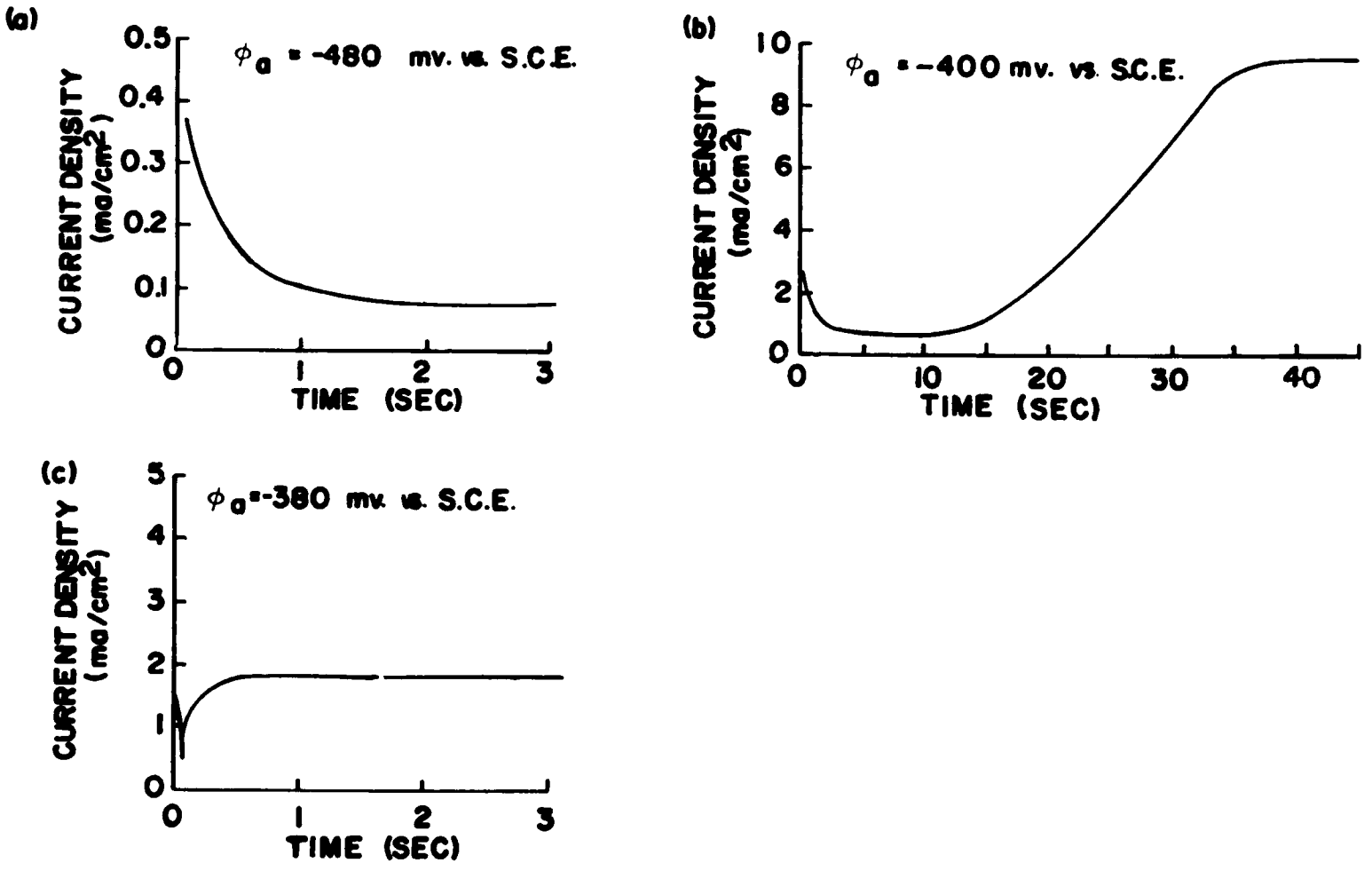

Figure 6. Typical Current Transients during Potentiostatic Polarization of Iron in 0.01M NaCl + 4.48M $NaClO_4$ + 0.01M $HClO_4$ Solutions.

C. Effect of Chloride Ions on the Anodic Dissolution of Iron in Highly Acidic Solutions (xM $HClO_4$ + yM HCl solutions with x + y = 4.5).

1. Corrosion potentials

Table 3 lists the observed steady state corrosion potentials, which varied little for Cl^- < 0.03 M and shifted to more active potentials with increase in chloride concentration.

2. Polarization behavior

Steady state anodic potentiostatic polarization of iron is shown in Figures 7 and 8. In pure perchlorate solution, (Cl^-) = 0.0M, an anodic Tafel slope of 44 mv/dec was observed. With increasing chloride concentration up to 0.05 M, the Tafel slope increased continuously from 44 mv/dec to nearly 100 mv/dec with increase in chloride concentration (Figure 7). The dissolution rate decreased with increasing chloride concentration.

In solutions with (Cl^-) > 0.05M, Tafel slopes were 100 mv/dec as shown in Figure 8. However, for (Cl^-) between 0.1 - 0.4 M, 40 mv/dec Tafel slopes were also obtained at higher polarization (φ_a > -250 mv vs S.C.E.) and no significant chloride effect was observed in this region. On the other hand, in the 100 mv/dec Tafel slope regions it was observed that the dissolution rate increased with the increase in chloride concentration in constant to results obtained for $(Cl^-) \leq 0.05$ M.

3. Corrosion rates

The corrosion currents are presented in Table 3. The corrosion currents decreased with increase in chloride concentration for (Cl^-) < 0.1 M. In greater concentrations the corrosion current increased rapidly with further increase in chloride concentration and followed the relationship, $\frac{\partial \log i_{corr}}{\partial \log (Cl^-)} \approx 1.1$.

TABLE 3. Effect of Cl^- on iron dissolution in 4.5 M H^+ solutions.

Electrolytes	φ_{corr} (mv vs SCE)	Anodic Tafel Slope (mv/dec)	i_{corr} (ma/cm^2)
4.5M $HClO_4$	-353± 5	44± 4	0.46
4.5M $HClO_4$ + 0.001M HCl	-364± 7	53± 5	0.25
4.5M $HClO_4$ + 0.003M HCl	-357± 5	74± 5	0.32
4.49M $HClO_4$ + 0.01M HCl	-351± 6	79± 4	0.31
4.473M $HClO_4$ + 0.027M HCl	-353± 5	90± 5	0.28
4.45M $HClO_4$ + 0.05M HCl	-364± 6	96± 5	0.18
4.4M $HClO_4$ + 0.1M HCl	-375± 6	95± 4	0.10
4.3M $HClO_4$ + 0.2M HCl	-387± 6	93± 5	0.18
4.1M $HClO_4$ + 0.4M HCl	-390± 10	100± 5	0.29
3.5M $HClO_4$ + 1.0M HCl	-381± 5	100± 5	1.38
2.5M $HClO_4$ + 2.0M HCl	-375± 6	101± 5	2.70
1.5M $HClO_4$ + 3.0M HCl	-382± 10	103± 5	4.05
0.5M $HClO_4$ + 4.0M HCl	-390± 9	105± 5	4.95

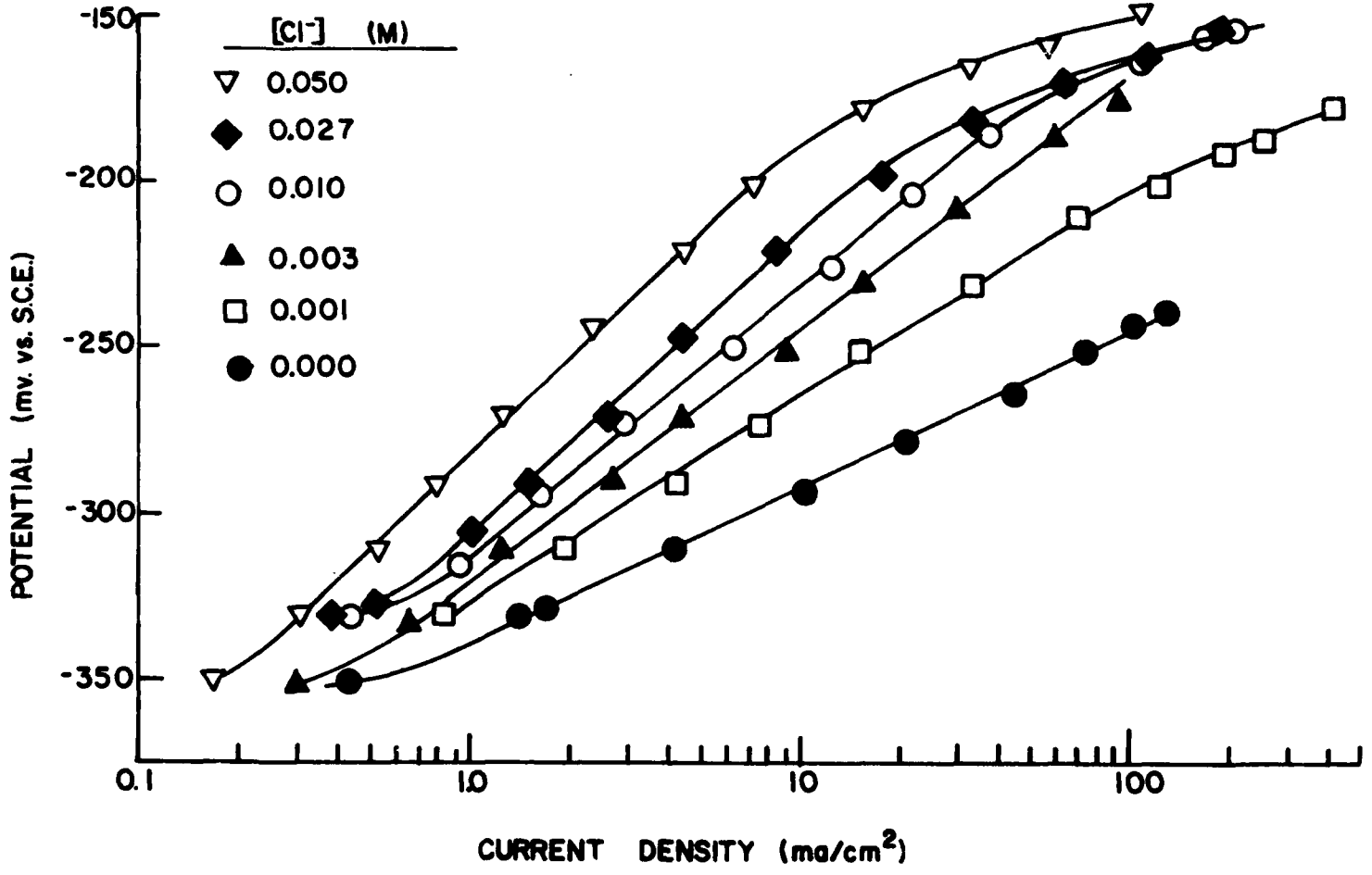

Figure 7. Anodic Dissolution of Iron in 4.5M $HCl-HClO_4$ Solutions; $(Cl^-) \leq 0.05M$.

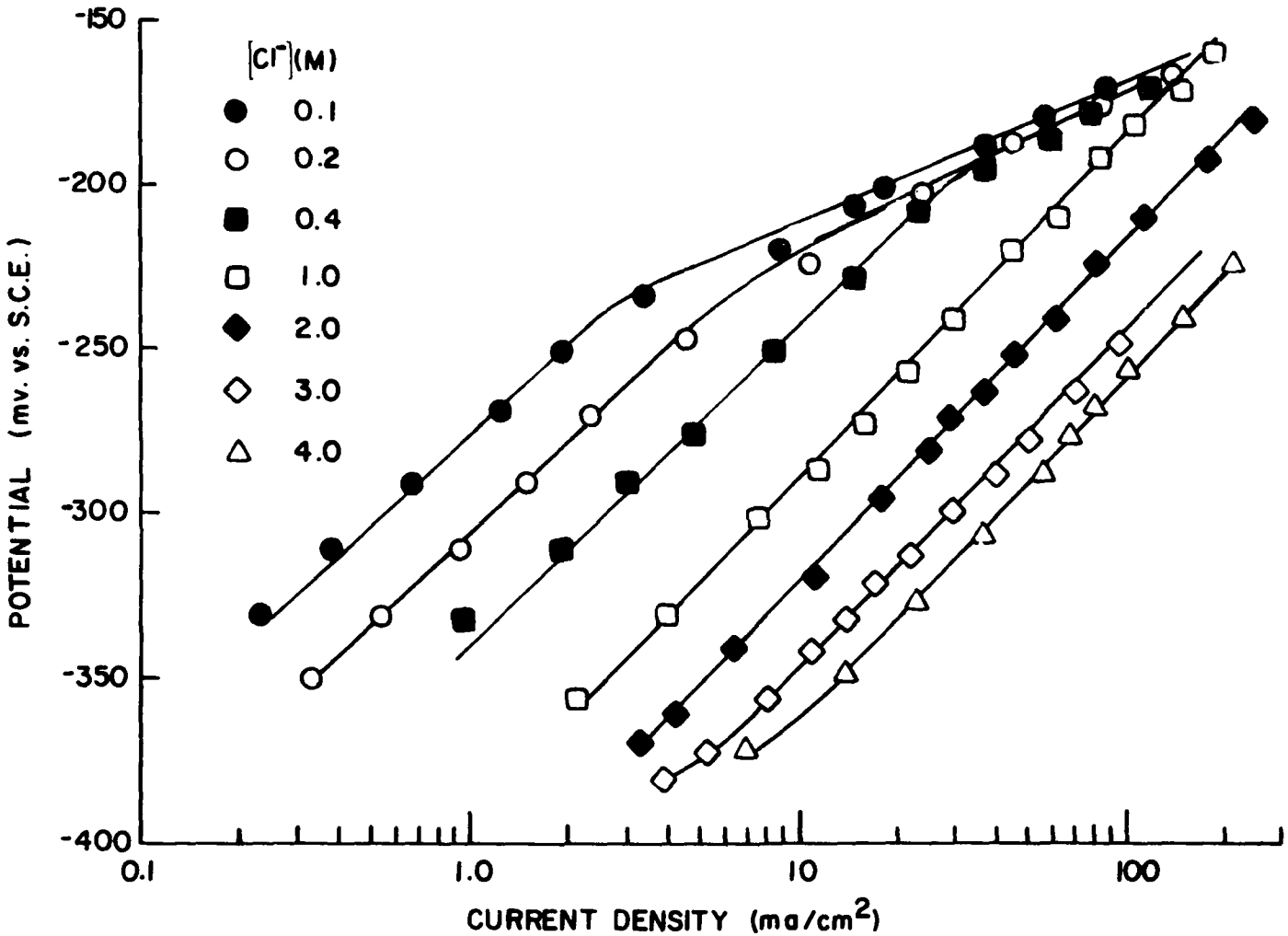

Figure 8. Anodic Dissolution of Iron in 4.5M $HCl-HClO_4$ Solutions; $0.1M \leq (Cl^-) \leq 4M$.

DISCUSSION

Low (H^+) - High (Cl^-) Solutions

As shown in Figures 1, 4 and 5, anodic Tafel slopes of about 78 mv/dec were obtained for iron dissolution in solutions with $(H^+) < 0.5$ M and $(Cl^-) > 0.01$M at low polarization; at high polarization the Tafel slope changed to 40 mv/dec. The change in the anodic Tafel slope from about 70 $\pm$ 10 mv/dec to a smaller value at higher polarization was also observed by Schwabe and Voigt for HCl-KCl and H_2SO_4-KCl solutions (7), and by Chin and Nobe for the NaCl-$NaClO_4$-0.1M $HClO_4$ solution (6).

Figure 9 is a reaction order plot with respect to Cl^- for the 78 mv/dec Tafel slope region in Figure 5 and shows that

$$\left(\frac{\partial \log i_a}{\partial \log [Cl^-]}\right)_{pH,\ \varphi} = 0.4$$

Figure 10 is the reaction order plot of iron dissolution with respect to pH from the data in Figure 1 and shows that

$$\left(\frac{\partial \log i_a}{\partial\ pH}\right)_{[Cl],\ \varphi} \approx 0.6$$

In the high polarization region, Figure 5 shows that iron dissolution is independent of (Cl^-); on the other hand, Figure 11 (plot of data in Figure 1) shows that

$$\left(\frac{\partial \log i_a}{\partial\ pH}\right)_{[Cl^-],\ \varphi} \approx 1.1$$

In summary, the rate of iron dissolution in concentrated chloride solution with $(H^+) < 0.5$ M can be expressed as

$$i_a = K_a\ (Cl^-)^{0.4}\ (OH^-)^{0.6}\ \exp\left(\frac{3\ F\ \varphi}{4\ RT}\right) \qquad (1)$$

at low polarization, and

$$i_a = K_a'\ (OH^-)^{1.1}\ \exp\left(\frac{3F\varphi}{2RT}\right) \qquad (2)$$

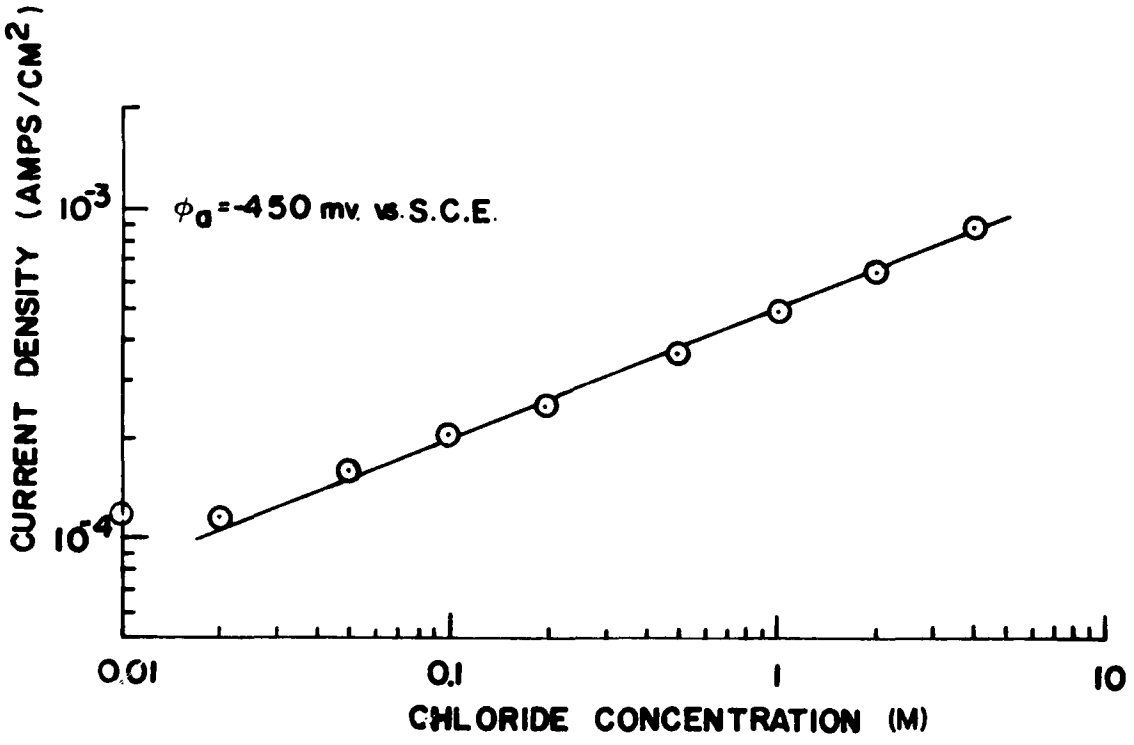

Figure 9. Reaction Order Plot of Iron Dissolution with respect to (Cl^-) in xM NaCl + yM $NaClO_4$ + 0.01M $HClO_4$ (x+y = 4.49) Solutions. Low Polarization Region.

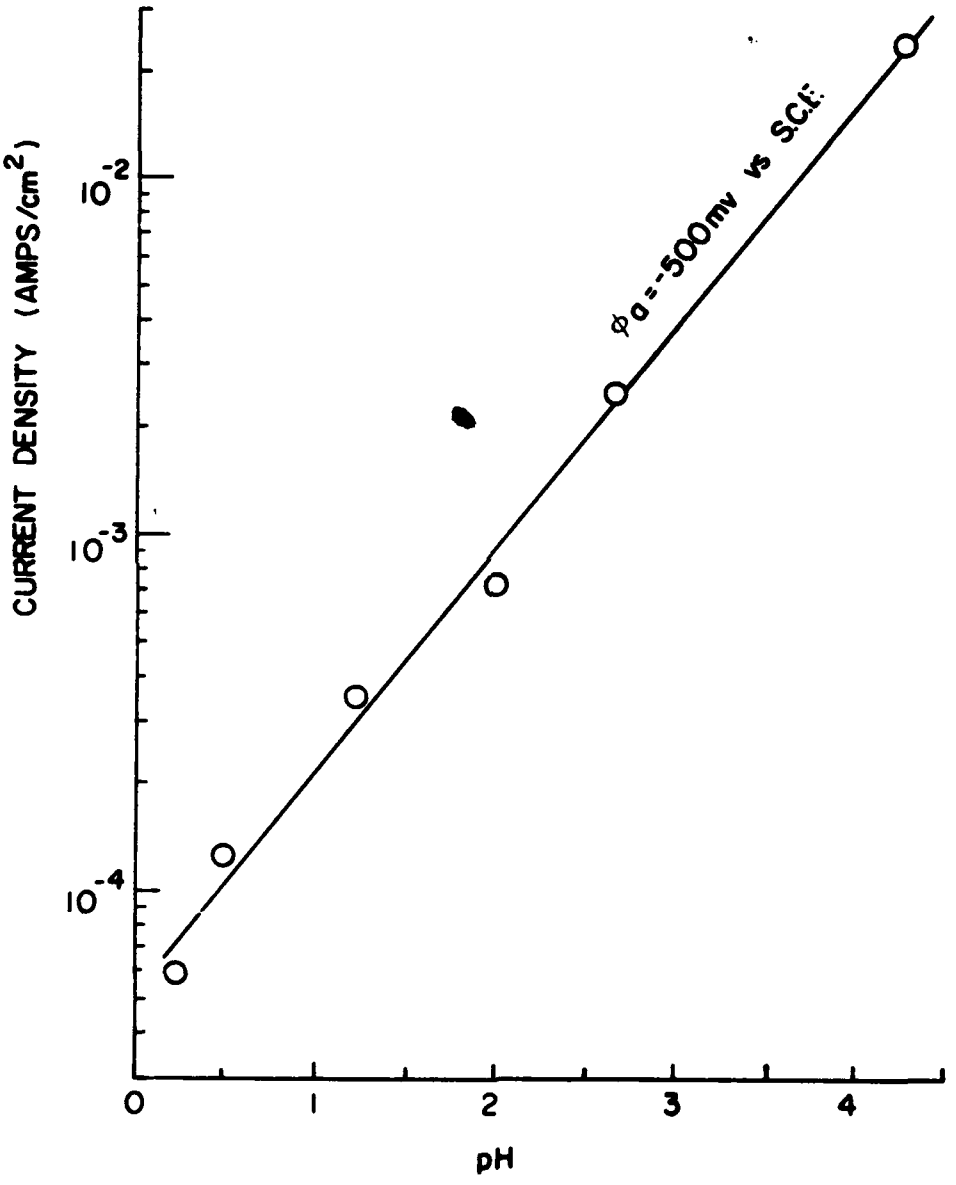

Figure 10. Reaction Order Plot of Iron Dissolution with respect to pH in 4.5 M HCl-NaCl Solutions; Low Polarization Region.

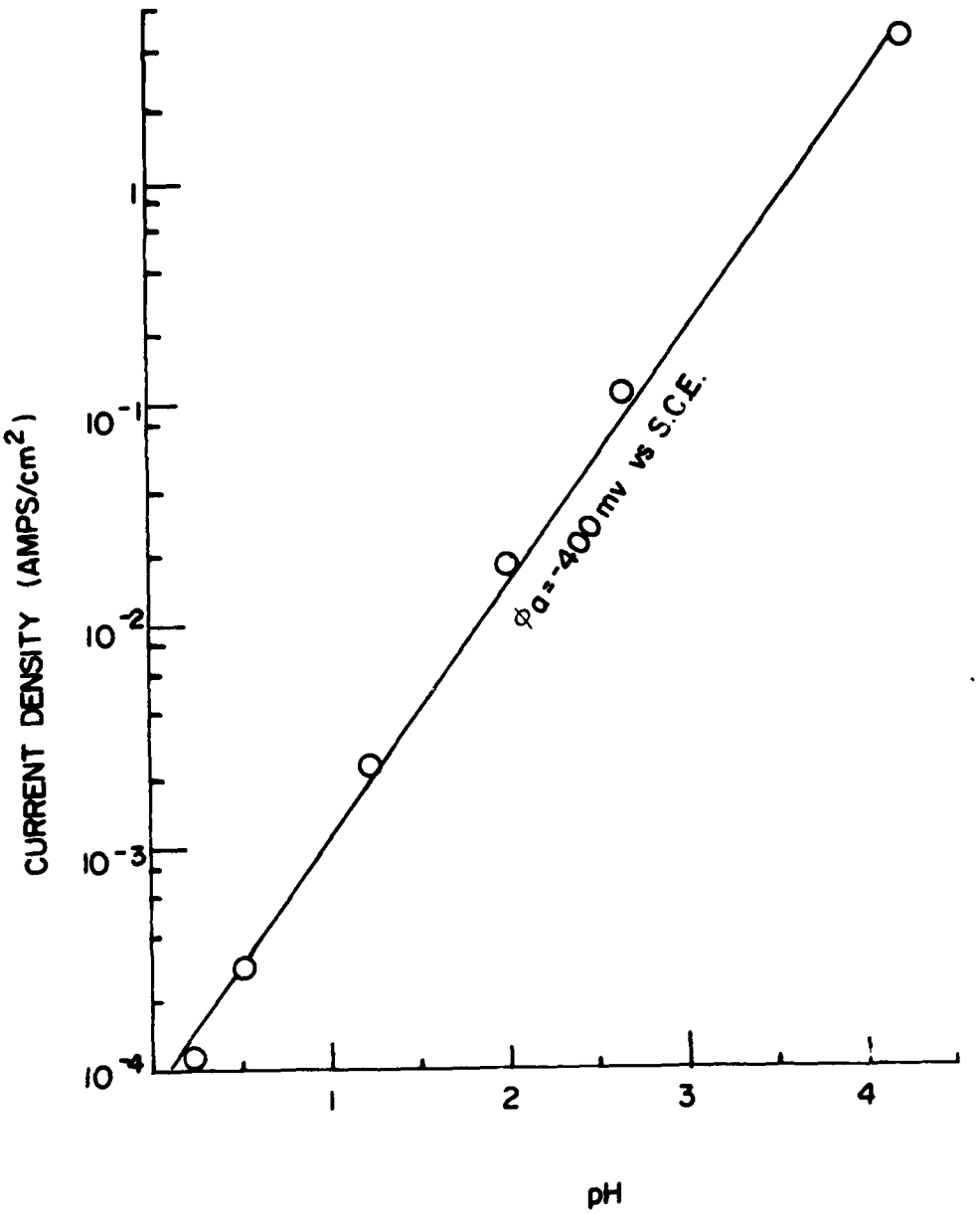

Figure 11. Reaction Order Plot of Iron Dissolution with respect to pH in 4.5M HCl-NaCl Solutions: High Polarization Region.

Equation (1) is in accord with results reported previously (6). The positive reaction order with respect to chloride ion concentration also agreed with Kolotyrkin et al (10) and Altukhov et al (11) for iron dissolution in Na_2SO_4 and KCl solutions (pH = 3). Both observed $\left(\frac{\partial \log i_a}{\partial \log (Cl^-)}\right)_{\varphi, pH} \approx 0.6$ for $0.01M < (Cl^-) < 0.1$ M. In contrast, inhibition of iron dissolution by chloride ions has been reported by Lorenz et al (3,4) and Schwabe and Voigt (7) for Na_2SO_4 + KCl solutions and by McCafferty and Hackerman (9) for 0.2M HCl + xM LiCl solutions (x varied from 1-6). Lorenz et al (3,4) report

$$i_a = k_a (Cl^-)^{-0.7} (OH^-) \exp\left(\frac{F\varphi}{RT}\right), \quad 0.1\ M \leq (Cl^-) \leq 2.0M \qquad (3)$$

McCafferty and Hackerman report that

$$i_a = k_a (Cl^-)^{-0.85} (OH^-)^{0.9} \exp\left(\frac{0.9F\varphi}{RT}\right), \quad 1M < (Cl^-) < 6M, (H^+) = 0.2M \qquad (4)$$

In order to determine the effect of one species on the rate of reaction, the activities of all other electro-active species must be kept constant while varying the activity of the species of interest. The mean activity coefficient of an ion in a mixed electrolyte depends strongly on the total ionic strength of the solutions (12 - 14). None of the above mentioned investigations, except Chin and Nobe (6), maintained the total ionic strength of their solutions constant.

The experimental results of iron dissolution in low (H^+) - high (Cl^-) solutions can be interpreted by coupling the chloride-accelerated mechanism (6) with the Bockris mechanism (12),

Chloride-accelerated mechanism

step 1: $Fe + H_2O + Cl^- \underset{-1}{\overset{+1}{\rightleftharpoons}} Fe(ClOH)^-_{ads} + H^+ + e$

step 2: $Fe(ClOH)^-_{ads} \underset{-2}{\overset{+2}{\rightleftharpoons}} Fe(ClOH) + e$

step 3: $Fe(ClOH) + H^+ \underset{-3}{\overset{+3}{\rightleftharpoons}} Fe^{++} + Cl^- + H_2O$

Bockris mechanism

step 1': $Fe + H_2O \underset{-1'}{\overset{+1'}{\rightleftharpoons}} Fe(OH)_{ads} + H^+ + e$

step 2': $Fe(OH)_{ads} \underset{-2'}{\overset{+2}{\rightleftharpoons}} Fe(OH)^+ + e$

step 3': $Fe(OH)^+ + H^+ \underset{-3'}{\overset{3'}{\rightleftharpoons}} Fe^{++} + H_2O$

Step 2 and step 2' are assumed to be the rate determining steps.

It is assumed that the Temkin adsorption isotherm applies to the surface coverage of $(FeClOH)^-$. Similar to the derivation given previously (6) the rate of step 2 can be expressed as

$$r_2 = k_2 \theta_{(FeClOH)^-} \frac{(Cl^-)^{1-\gamma_2}}{(H^+)^{1-\gamma_2}} \frac{(1-\theta_T)^{1-\gamma_2}}{\theta^{1-\gamma_2}_{(FeClOH)^-}} \exp \frac{(\beta_2 + 1 - \gamma_2)F\varphi}{RT} \qquad (5)$$

where θ_T is the total surface coverage (exclusive of H_2O) and β_2 and γ_2 are the symmetry factors for step 2.

Since $0.2 < \theta_{Fe(ClOH)^-} < 0.8$ and if $\theta_{FeOH} << \theta_{Fe(ClOH)^-}$, then $\theta_T \approx \theta_{Fe(ClOH)^-}$ and the term $\left(\frac{1-\theta_T}{\theta_{Fe(ClOH)^-}}\right)^{1-\gamma_2}$ is essentially constant. By assuming $\beta_2 = 0.4$ and $\gamma_2 = 0.6$, the dissolution rate contributed by the chloride-catalyzed mechanism is given by

$$i_{a,Cl} = k_{a,Cl} \theta_{Fe(ClOH)^-} (Cl^-)^{0.4} (OH^-)^{0.4} \exp\left(\frac{0.8F\varphi}{RT}\right) \qquad (6)$$

For the reaction steps 1', 2' and 3', the free energy of adsorption of FeOH can be expressed as

$$\Delta G^o_{\theta,FeOH} = \Delta G^o_{0,FeOH} - f_{FeClOH^-} RT\theta_{FeClOH^-} - RT\theta_{FeOH} \qquad (7)$$

where $\Delta G^o_{0,FEOH}$ is the standard free energy of adsorption on the bare surface. Since the standard free energy of adsorption of FeOH should be much higher than that of $Fe(ClOH)^-$ and θ_{FeOH} is very small, $\Delta G^0_{\theta,FeOH} \approx \Delta G^0_{0,FeOH}$. This result indicates that FeOH can be assumed to follow Langmuir adsorption behavior. The rate of step 2' is

$$r_{2'} = k_{2'} (1-\theta_T) (OH^-) \exp \frac{(1+\beta_{2'})F\varphi}{RT} \qquad (8)$$

With $\theta_T \approx \theta_{Fe(ClOH)^-}$ and $\beta_{2'} = 0.5$ the rate of the anodic dissolution contributed by the Bockris mechanism can be expressed as

$$i_{a,OH} = k_{a,OH} (1 - \theta_{Fe(ClOH)^-}) [OH^-] \exp\left(\frac{3F\varphi}{2RT}\right) \qquad (9)$$

The total dissolution rate is then

$$i_a = i_{a,Cl} + i_{a,OH}$$

$$= k_{a,Cl}\,\theta_{Fe(ClOH)^-}\,(Cl^-)^{0.4}\,(OH^-)^{0.4}\exp\left(\frac{0.8F\varphi}{RT}\right)$$

$$+ k_{a,OH}\,(1-\theta_{Fe(ClOH)^-})\,(OH^-)\,\exp\left(\frac{3F\varphi}{2RT}\right) \qquad (10)$$

At lower potentials, the dissolution rate by the chloride-acccelerated mechanism is dominant, i.e., $i_{a,Cl} >> i_{a,OH}$. By assuming the adsorption of $\theta_{Fe(ClOH)^-}$ is nearly constant in concentrated chloride solutions,

$$i_{a,Cl} \approx k'_{a,Cl}\,(Cl)^{0.4}\,(OH^-)^{0.4}\exp\left(\frac{0.8\,F\varphi}{RT}\right) \qquad (11)$$

which is in good agreement with the experimental data at low polarization.

At higher potentials the rate of dissolution by the Bockris' mechanism is predominant.

$$i_{a,OH} \approx k'_{a,OH}\,(OH^-)\,\exp\left(\frac{3\,F\varphi}{2RT}\right) \qquad (12)$$

which agrees well with the experimental data at high polarization.

The schematic diagram of Figure 12 shows that the apparent total current density is the sum of the two partial current densities $i_{a,OH}$ and $i_{a,Cl}$. At the transition potential, E_t, the two partial current densities are equal, i.e., $i_{a,OH} = i_{a,Cl} = i_t$. Equations (11) and (12) give

$$\frac{\partial E_t}{\partial\, pH} = -42 \quad mv$$

and

$$\frac{\partial \log i_t}{\partial\, pH} = 0.14$$

which are in good agreement with the observed values of -38 mv and 0.16, respectively. Although the coupling of the chloride-accelerated mechanism with the Bockris' mechanism has been suggested earlier (6), the experimental

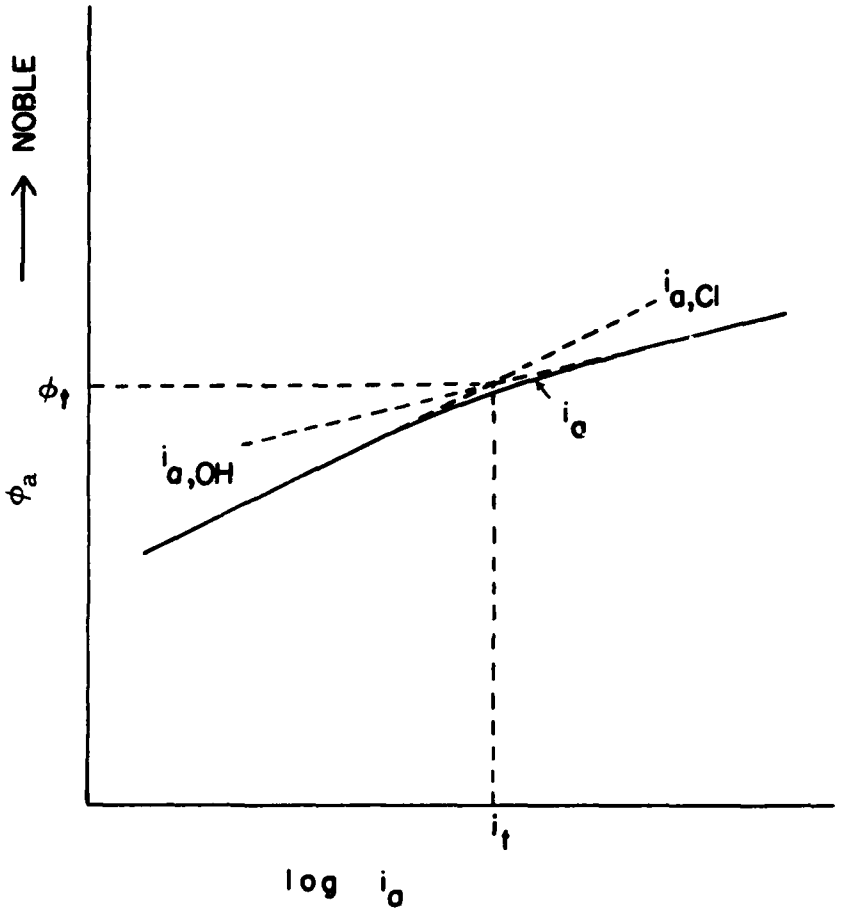

Figure 12. Schematic Diagram for OH^- -Accelerated and Cl^--Accelerated Anodic Dissolution of Iron.

results of that study were not sufficient for confirmation. However, the results of this study clearly confirm the previous suggestion.

Low (H^+) - Low (Cl^-) Solutions

In above analysis for concentrated chloride solutions it is assumed that the surface coverage of the intermediate, $Fe(ClOH)^-$ is in the range of $0.2 < \theta < 0.8$. However, in very low chloride concentration solutions the surface coverage of $Fe(ClOH)^-$ should be much lower than that expected in concentrated chloride solution and $(1-\theta)_{(FeClOH)^-} \approx 1$ and iron dissolution should follow the Bockris' mechanism,

$$i_a \approx k_{a,OH} (OH^-) \exp\left(\frac{3F\varphi}{2RT}\right)$$

A 40 mv/dec Tafel slope is obtained as shown in Figure 3 for iron dissolution in solutions of pH = 1.07 and $(Cl^-) < 10^{-3}$ M. With increase in (Cl^-) from 10^{-3} to 10^{-2} M, the rate of iron dissolution decreases. This inhibition effect is probably due to the decrease in the number of active sites for iron dissolution by the Bockris' mechanism as the result of competitive adsorption of Cl^- and OH^- when the (Cl^-) is increased from 10^{-3} to 10^{-2} M. However, since the surface coverage of Cl^- is still very low, iron dissolution by the chloride-accelerated reaction is not appreciable.

High (H^+) - High (Cl^-) Solutions

For $(H^+) \geq 1$ M, and $(Cl^-) \geq 0.05$M, an anodic Tafel slope of 115 mv/dec was obtained (Figure 8), which implies that the dissolution mechanism is different than that in solutions of lower (H^+).

Figures 13 and 14 show the reaction order plots of iron dissolution in highly acidic-concentrated chloride solutions with respect to H^+ and Cl^-, respectively.

$$\frac{\partial \log i_a}{\partial \log (H^+)} = 1.0$$

$$\frac{\partial \log i_a}{\partial \log (Cl^-)} = 1.1$$

The reaction order of iron dissolution with respect to activity of H^+ is shown in Figure 15,

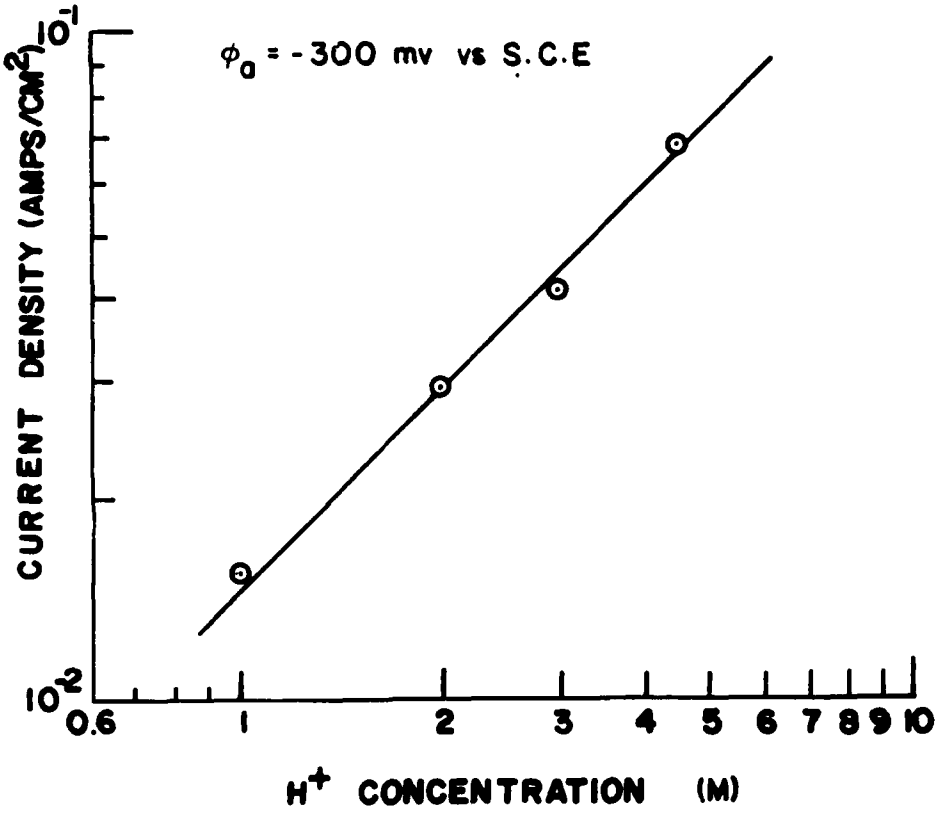

Figure 13. Reaction Order Plot of Iron Dissolution with respect to (H^+) in Highly Acidic 4.5M NaCl-HCl Solutions.

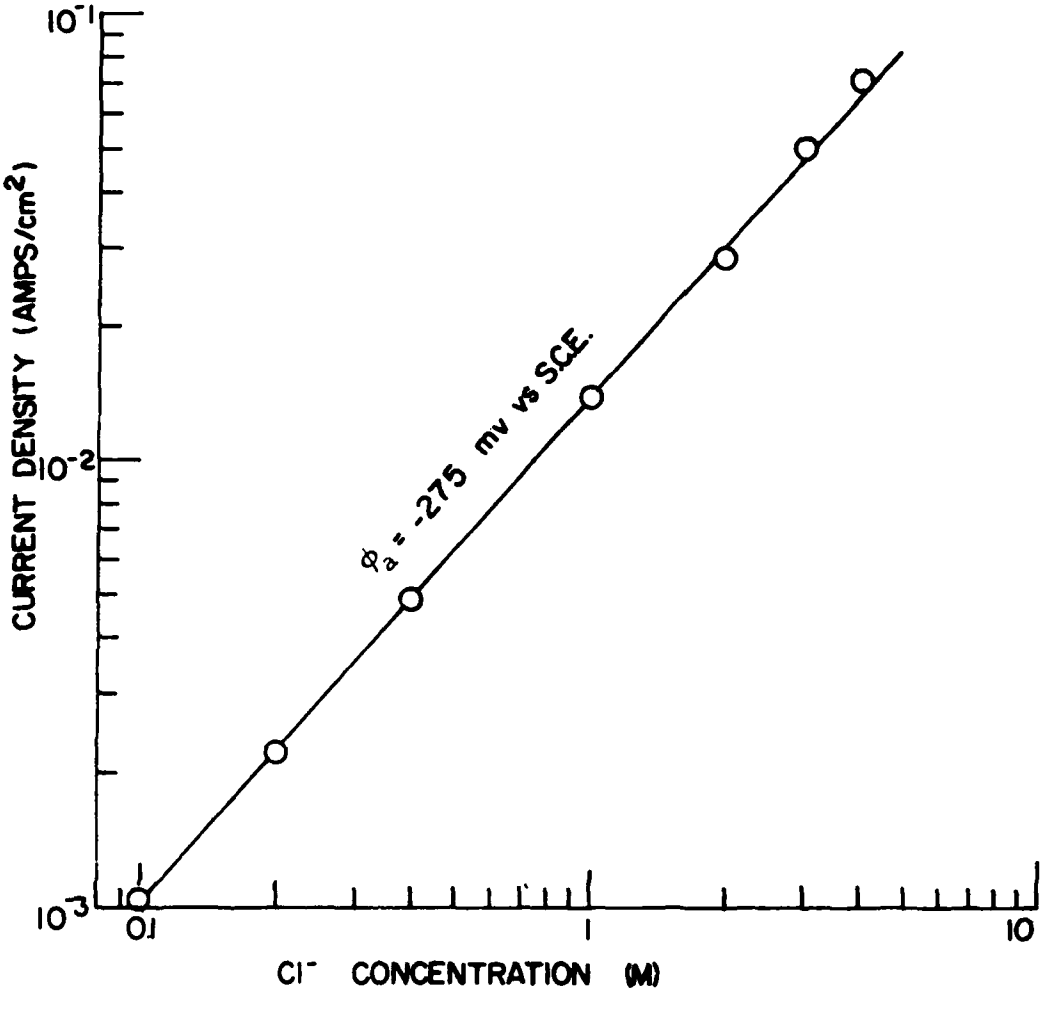

Figure 14. Reaction Order Plot of Iron Dissolution with respect to (Cl^-) 4.5M HCl-$HClO_4$ Solutions.

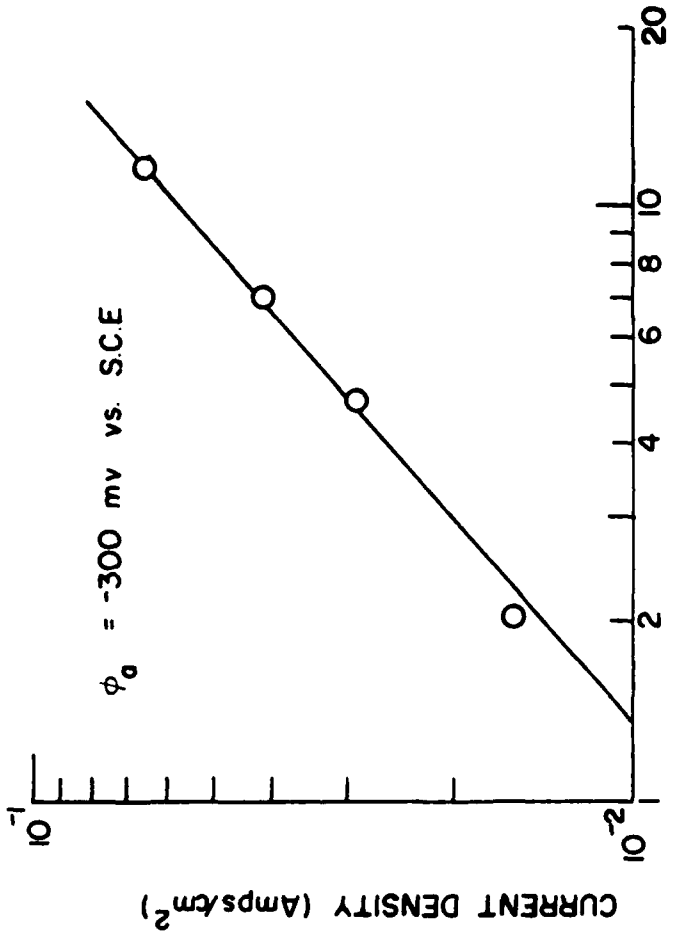

Figure 15. Reaction Order Plot of Iron Dissolution with respect to (H^+) in Highly Acidic 4.5M NaCl-HCl Solutions.

$$\frac{\partial \log i_a}{\partial \log [H^+]} = 0.9$$

where $[H^+] = \gamma_{\pm} m_{H^+}$. Thus, the experimental rate of iron dissolution is given by

$$i_{a,H} = k_{a,H} [H^+]^{0.9} (Cl^-)^{1.1} \exp\left(\frac{F\varphi}{2RT}\right) \qquad (13)$$

At high polarization with (Cl^-) varying from 0.05 M to 0.4M, the Tafel slope changes to 40 mv/dec similar to that observed for the low (H^+) solutions. The polarization current in this 40 mv/dec Tafel region was essentially independent of (Cl^-).

Anodic Tafel slopes of 100 mv/dec and + 1 reaction orders with respect to activity of H^+ have been reported by Darwish et al (8), for iron dissolution in highly acidic-concentrated chloride solution (5M NaCl - HCl) with $(H^+) > 1M$ and $(Cl^-) \geq 0.5$ M. However, they reported a + 0.6 reaction order with respect to Cl^-.

McCafferty and Hackerman (9), who studied iron dissolution in LiCl + HCl solutions, have also reported positive reaction orders with respect to activity of H^+. However, they obtained an H^+ reaction order of + 2 for 6 M Cl^- with $(H^+) > 2.4$ M. Their Cl^- reaction order was between + 0.6 to 0.9, and the anodic Tafel slope was about 70 mv/dec.

In highly acidic solutions the rate of step 2 of the chloride-accelerated mechanism will be greatly decreased since $\theta_{(FeClOH)^-}$ will become very small. In light of the experimental results of this study the following mechanism is proposed for iron dissolution in highly acidic-concentrated chloride solutions.

step 1'': $Fe + Cl^- \rightleftharpoons (FeCl)_{ads} + e$

step 2'': $(FeCl)_{ads} + H^+ \rightleftharpoons (FeClH)^+_{ads}$

step 3'': $(FeClH)^+_{ads} + Cl^- \longrightarrow FeCl_2 + H^+ + e$

step 4'': $FeCl_2 \rightleftharpoons Fe^{++} + 2\,Cl^-$

By assuming that step 3'' is the rate determining step and $\theta_{FeCl} \approx 1$, with the adsorbed intermediates following Langmuir adsorption, the following rate equation can be derived for step 3''

$$r_{3''} = k_{3''} \theta_{FeClH^+} (Cl^-) \exp\left(\frac{\beta_{3''} F\varphi}{RT}\right) \quad (14)$$

Since step 2'' is in quasi-equilibrium, an expression for $\theta_{(FeClH)^+}$ can be obtained and

$$i_{a,H} = k_{a,H} (Cl^-) (H^+) \exp\left(\frac{\beta_{3''} F\varphi}{RT}\right) \quad (15)$$

With $\beta_{3''} = 0.5$, the rate of the iron dissolution for H^+ accelerated mechanism is:

$$i_{a,H} = k_{a,H} (Cl^-) (H^+) \exp\left(\frac{F\varphi}{2RT}\right) \quad (16)$$

This equation is in good agreement with the experimental results (Equation 13).

In Figure 8 it is shown that by increasing the (Cl^-) from 0.1 M to 4M, iron dissolution is increased. The anodic Tafel remains constant at about 100 mv/dec indicating that the mechanism of iron dissolution remains the same in this higher range of (Cl^-). Figure 8 shows that above about -200 mv vs SCE and (Cl^-) between 0.1 - 0.4 M, iron dissolution tends to a Tafel line which is independent of (Cl^-) with a slope of about 40 mv/dec. Although the polarization data above -200 mv vs S. C. E. are not complete for all (Cl^-) studied, the results obtained are sufficient to suggest that iron dissolution in highly acidic chloride solutions follows the combined H^+ - accelerated and Bockris mechanism. That is

$$i_a = k_{a,OH} (OH^-) \exp\left(\frac{3F\varphi}{2RT}\right) + k_{a,H} (H^+) (Cl^-) \exp\left(\frac{F\varphi}{2RT}\right) \quad (17)$$

At high enough (Cl^-) and low polarization

$$i_a \approx i_{a,H}$$

At high enough (Cl^-) and high polarization,

$$i_a \approx i_{a,OH}$$

High (H^+) - Low (Cl^-) Solutions

A careful examination of Figures 7 and 8 shows the following interesting and important phenomena. Figure 7 shows that in the complete absence of Cl^- an anodic Tafel slope of 40 mv/dec is obtained which indicates iron dissolution in (H^+)=4.5M by the Bockris mechanism. With the addition of small

amounts of Cl^- to 0.05 M, the rate of iron dissolution decreases with increase in (Cl^-); that is, Cl^- inhibits iron dissolution in the low concentration range of Cl^- in highly acidic solutions. This phenomenon was also observed in low (H^+) solutions (pH $\geq$ 1). Figure 7 also shows that the anodic Tafel slope is increased by increasing the (Cl^-) with about 100 mv/dec Tafel slope obtained for iron in 0.05M Cl^-. This result indicates that the mechanism of iron dissolution is changing when the (Cl^-) is increased from 0.00 - 0.05M.

In solutions of very low chloride ion concentrations the surface coverage of FeCl is probably very low, and the Bockris mechanism is dominant. However, since part of the surface is covered with adsorbed FeCl, and if $\vartheta_{FeCl} >> \theta_{FeOH}$,

$$i_a \approx k_{a,OH} (1-\theta_{FeCl}) (OH^-) \exp\left(\frac{3F\varphi}{2RT}\right) \tag{18}$$

By assuming Langmuir adsorption and that step 1'' is at quasi-equilibrium.

$$k_{1''}(Cl^-)(1-\vartheta_{FeCl}) \exp\frac{(1-\beta_{1''})F\varphi}{RT} = k_{-1''}\theta_{FeCl} \exp -\frac{\beta_{1''} F\varphi}{RT}$$

where $\vartheta_{FeCl} \rightarrow 0$, but $\theta_{FeCl} >> \theta_{FeOH} + \theta_{(FeClH)^+}$. Then

$$\vartheta_{FeCl} = \frac{k_{1''}(Cl^-) \exp\left(\frac{F\varphi}{RT}\right)}{k_{1''}(Cl^-) \exp\left(\frac{F\varphi}{RT}\right) + k_{-1''}} \tag{19}$$

and

$$1-\vartheta_{FeCl} = \frac{1}{K_{1''}(Cl^-) \exp\left(\frac{F\varphi}{RT}\right) + 1} \tag{20}$$

where $K_{1''} = \frac{k_{1''}}{k_{-1''}}$.

By substituting Equation (20) into Equation (18),

$$i_a = k_{a,OH}\left(\frac{(OH^-) \exp\left(\frac{3F\varphi}{2RT}\right)}{1 + K_{1''}(Cl^-) \exp\left(\frac{F\varphi}{RT}\right)}\right) \tag{21}$$

In chloride-free solution, equation (21) gives

$$i_a = k_{a,OH} (OH^-) \exp\left(\frac{3F\varphi}{2RT}\right)$$

which gives 40 mv/dec Tafel slopes. In the presence of small amounts of chloride ions and with $K_{1''}(Cl^-)\exp(\frac{F\varphi}{RT}) >> 1$, Equation (21) gives

$$i_a \approx k_{a,OH} K_{1''}^{-1} (Cl^-)^{-1} (OH^-) \exp\left(\frac{F\varphi}{2RT}\right) \tag{22}$$

which gives 120 mv/dec Tafel slope. However, in low chloride-containing solutions between the above two limiting cases, Equation (20) can be written as

$$1-\theta_{FeCl} \approx K_{1''}^{-\delta} (Cl^-)^{-\delta} \exp\left(-\frac{\delta F \varphi}{RT}\right) \tag{23}$$

where $0 \leq \delta \leq 1$ and δ changes from 0 to 1 with increasing (Cl^-). By substituting Equation (23) into Equation (18),

$$i_a \approx k_{a,OH} K_{1''}^{-\delta} (Cl^-)^{-\delta} (OH^-) \exp\left(\frac{(\frac{3}{2} - \delta) F\varphi}{RT}\right) \tag{24}$$

Since δ changes from 0 to 1 with increasing chloride concentration, Equation (24) shows the inhibition effect of Cl^- and the change in the Tafel slope from 40 to 120 mv/dec with increasing chloride concentration which is in good agreement with the experimental results shown in Figure 7 for 0.00 to 0.05M Cl^- solutions.

REFERENCES

1. Foley, R.T. Corr., 26, 58, (1970).

2. Szklarska-Smialowska, Z. Corr., 27, 223, (1971).

3. Lorenz, W.J., H. Yamaoka and H. Fischer. Ber. Bun. Phy. Chem., 67, 932, (1963).

4. Lorenz, W.J., Corr. Sci., 5, 121, (1965).

5. Kolotyrkin, Ya.M. Prot. of Met., 3, 101, (1967).

6. Chin, R.J. and K. Nobe. J. Electrochem. Soc., 119, 1457, (1972).

7. Schwabe, K. and C. Voigt. Electrochim. Acta, 14, 853, (1969).

8. Darwish, N.A., F. Hilbert, W.J. Lorenz and H. Rosswag. Electrochin. Acta. 18, 421 (1973).

9. McCafferty, E. and N. Hackerman. J. Electrochem. Soc., 119, 999, (1972).

10. Golovina, G.V., G.M. Florianovich and Ya. M. Kolotyrkin. Prot. Met., 2, 34, (1966).

11. Altukhov, V.K. and I.K. Marshakov. Soviet Electrochem., 7, 1132, (1970).

12. Bockris, J. O'M., D. Drazic and A.R. Despic. Electrochim. Acta, 4 325, (1961).

PART III

WORK PERFORMED UNDER THE SUPERVISION OF DIETER LANDOLT, 1970-1973

The research performed was aimed at the elucidation of metal dissolution processes under conditions of high anodic potentials where metals are usually covered by anodic films. The fundamental knowledge created is relevant to electrochemical metal working processes and certain types of corrosion such as pitting corrosion.

During the contract period, the author and his coworkers studied the following topics: transpassive behavior of nickel in sodium chlorate electrolytes in the presence and absence of sodium chloride; development of experimental techniques suited for high rate electrolysis studies; transpassive behavior of nickel in concentrated sulfuric acid; high rate dissolution of nickel in sodium nitrate; anodic layer formation and mass transport processes during anodic dissolution of iron in chloride electrolytes.

Results of this research have been published in the scientific literature and in the form of theses and technical reports. A list is given in the appendix. In the following, a brief summary of the more important results is given:

The current efficiency for transpassive metal dissolution in $NaClO_3$ and $NaNO_3$ electrolytes is an increasing function of current density. The anode potential under these conditions follows approximate Tafel behavior up to current densities of at least 10 A/cm^2. The two observations permit one to understand why so called passivating electrolytes in electrochemical machining give a better dimensional accuracy than non passivating types.

Surface texture resulting from transpassive dissolution is intimately related to mass transfer processes in the electrolyte solution. This conclusion was drawn in a preliminary way from the studies of nickel dissolution in $NaNO_3$ and H_2SO_4 electrolytes. It has since been confirmed in a more quantitative way by investigations carried out by the author's group at the Swiss Federal Institute of Technology in Lausanne.

Anodic dissolution of iron in chloride media at high rate shows mass transfer limited currents resulting from the presence of a precipitated salt layer at the anode surface. In the absence of convection, salt precipitation leads to a sharp increase in anode potential due to the formation of an anodic film of high resistance.

M.S. Theses completed under the present contract:

M. Datta: "High Rate Anodic Nickel Dissolution in NaCl and $NaClO_3$." UCLA, 1971.

Y.R. Mehra: "Transpassive Dissolution of Nickel in Concentrated Sulfuric Acid Solutions," UCLA, 1972.

A.M. Bengali: "Effect of Chlorate Ion on Nickel Corrosion in Chloride Media," UCLA. 1972.

H.C. Kuo: "Anodic Film Formation of Iron in Concentrated Chloride Media," UCLA, 1973.

Papers published in the scientific literature:

M. Datta, D. Landolt: "Stoichiometry of Anodic Nickel Dissolution in NaCl and $NaClO_3$ under Active and Transpassive Conditions," Corrosion Science 13 (1973), 187-199.

D. Landolt: "Flowchannel Cell for High Rate Electrolysis Studies," Rev. Sci. Instr. 43 (1972), 592.

D. Landolt: "Throwing Power Measurements during Nickel Dissolution under Active and Transpassive Conditions," J. Electrochem. Soc. 119 (1972), 708.

H.C. Kuo, D. Landolt: "Rotating Disk Electrode Study of Iron Dissolution in Concentrated Chloride Media," Electrochimica Acta 1975 (in press).

A further publication with the tentative title: "Galvanostatic Transient Study of Anodic Film Formation on Iron in Concentrated Chloride Media," by H.C. Kuo and D. Landolt is in preparation.

Technical Reports:

Three ONR technical reports were mailed out. Their content corresponded to the titles: "High Rate Anodic Nickel Dissolution in NaCl and $NaClO_3$," "Flowchannel Cell for High Rate Electrolysis Studies" and "Throwing Power Measurements during Nickel Dissolution under Active and Transpassive Conditions" mentioned above.

Presentations at meetings:

D. Landolt: "Throwing Power of ECM Electrolytes under Active and Transpassive Dissolution Conditions," Electrochem. Soc. Meeting in Cleveland, October 1971.

A.M. Bengali, D. Landolt: "Corrosion of Nickel in the Presence of Sodium Chlorate," 1973 NACE Corrosion Research Conf., Anaheim, California, March 1973.

D. Landolt: "Metal Dissolution Mechanisms in ECM," First Int. Congress on Electrochemical Machining, Leicester, England, March 1973.

D. Landolt, H. C. Kuo: "Anodic Film Formation on Iron in Concentrated Chloride Media," 1975 NACE Corrosion Research Conference, Toronto, Canada, April 1975.